JOURNAL OF COMPUTATIONAL PHYSICS 115, 530–549 (1994)

Linear Stability of Resistive MHD Modes: Axisymmetric Toroidal Computation of the Outer Region Matching Data

A. PLETZER* AND A. BONDESON†

Centre de Recherches en Physique des Plasmas, Association Euratom—Confédération Suisse, Ecole Polytechnique Fédérale de Lausanne, 21, Av. des Bains, CH-1007 Lausanne, Switzerland

AND

R. L. DEWAR

Department of Theoretical Physics and Plasma Physics Laboratory, Research School of Physical Sciences and Engineering, The Australian National University, Canberra A.C.T. 0200, Australia

Received December 6, 1993

The quest to determine accurately the stability of tearing and resistive interchange modes in two dimensional toroidal geometry led to the development of the PEST-3 code, which is based on solving the singular, zero-frequency ideal MHD equation in the plasma bulk and determining the outer data Δ', Γ', and A' needed to match the outer region solutions to those arising in the inner layers. No assumptions regarding the aspect ratio, the number of rational surfaces or the pressure are made *a priori*. This approach is numerically less demanding than solving the full set of resistive equations and has the major advantage of allowing for non-MHD theories of the non-ideal layers. Good convergence is ensured by the variational Galerkin scheme used to compute the outer matching data. To validate the code, we focus on the growth rate calculations of resistive kink modes which are reproduced in good agreement with those obtained by the full resistive MHD code MARS.

1. INTRODUCTION

In tokamak plasmas, it is known that resistive magnetohydrodynamic (MHD) modes can provide disruptions [1] by allowing the formation of magnetic islands about rational, $q = m/n$ surfaces (where the magnetic field lines close after completing m turns in the toroidal and n turns in the poloidal directions). The $m = 2, n = 1$ mode is in particular effective in this respect. Resistive kink, $q = 1$ instabilities also appear to be involved in triggering sawtooth oscillations [2] in plasmas with central $q < 1$.

Resistive MHD modes are characterized by growth rates γ which scale as some fractional power $\geq \frac{1}{3}$ of the resistivity η. Provided η is sufficiently small so that the Lundquist number S defined as the ratio of resistive diffusion time to the characteristic Alfvén time is at least, say 10^6 (which is well fulfilled in large scale fusion experiments) one may then apply an asymptotic matching method [3] to describe these modes. This consists in dividing the plasma into an *outer region*, where both η and γ are negligible, and *inner layers* of small width $L \sim \eta^{1/3}$ containing the rational surfaces. All non-ideal effects are concentrated in the inner layers. The outer region and the inner layers give rise to solutions to be matched.

The asymptotic matching method was adopted by most analytic works on linear resistive modes, which predict that tearing modes are stable if the outer region matching quantity Δ' (≡ jump of the logarithmic derivative of the normal magnetic perturbation) is negative in the pressureless limit [4], or smaller than a positive threshold in the finite pressure case if the resistive interchange index $D_R < 0$, the plasma being resistive interchange unstable if $D_R > 0$. This result is due to Glasser, Greene, and Johnson [5], henceforth referred to as GGJ. Since these data can be entirely determined in the ideal region, the stability properties can be investigated without solving the higher order, inner layer equations. This is one advantage of the asymptotic matching method over the full resistive MHD approach, as used in MARS [6], for instance. The flexibility in the choice of physics in the inner layer also leaves the door open to study more complex non-ideal models, including weak rotation of the resonant surfaces [7, 8], diamagnetic rotation, trapped particles etc. A general formalism making no assumption as to the symmetry in the inner layer has been developed [9].

A major difficulty in computing the matching data remains, however, due to the presence of regular singularities of the outer region equation at the rational surfaces. They give rise to two distinct Frobenius solutions (i.e., with fractional power-like behaviour): the weakly singular *small solution* and the

* E-mail: alexandre.pletzer@crpp.epfl.ch.

† Present address: Theoretical Electrodynamics, Uppsala University, Box 534, S-751 21 Uppsala, Sweden.

0021-9991/94 $6.00

dominant *big solution* which is non-square integrable. The complete set of outer matching data is defined as the ratios of small to big solutions, involving all admissible tearing and interchange parities. Until recently, there was no algorithm capable of computing the outer matching data to sufficient accuracy so as to compete with the full resistive MHD code MARS. The solution to the accuracy problem was initiated by Miller and Dewar [10] who derived an integral expression for the outer matching data, based on the so-called "generalized Green's function" (GGF) method. This integral method is less sensitive to the pointwise accurate representation of the solutions, which is necessarily affected near the rational surfaces. The GGF scheme was extended and applied to cylindrical plasmas by Pletzer and Dewar [11], where the existence of a variational principle was found and was utilized to unveil symmetry relations among the outer matching data. The purpose of this paper is to apply this method to axisymmetric toroidal plasmas and to validate it by comparison with MARS results.

This paper is organized in the following way: the straight-field line coordinate system is presented in Section II. We review in Section III the derivation of the ideal marginal stability equation for the normal displacement field in the outer region. This equation can be regarded as a generalization of Newcomb's equation [12] to toroidal geometry. The Frobenius expansion of the small and big solutions about a rational surface is determined in Section IV. When the leading exponents of the singular solutions approach an integer, the big solution must be redefined. This situation, treated in Section V, occurs in particular when the pressure gradient vanishes at the rational surface. A global solution is constructed in Section VI from the approximate Frobenius solutions. The dominant part of the big solution is extracted analytically to become a driving term, and the remaining contribution captured by a finite element response function which bears the leading small solution behaviour (in addition to a regular solution). The outer matching data are defined in Section VII and extracted in Section VIII by means of the GGF method. Section IX focuses on the numerical implementation of the Galerkin finite element scheme, which also discusses the condition that the piecewise linear elements yield quadratic convergence for the matching data. In Section XI, we present careful comparisons between PEST-3 and MARS growth rate computations, for zero and finite pressure $n = 1$ resistive kink modes.

II. MAGNETIC FIELD LINE COORDINATES

We work in the non-orthogonal coordinate system (ψ, θ, ζ), where the equilibrium magnetic field lines

$$\mathbf{B} = \nabla\zeta \times \nabla\psi + q(\psi)\nabla\psi \times \nabla\theta \tag{1}$$

appear straight when graphed in the (θ, ζ) plane. That is, the *safety factor*

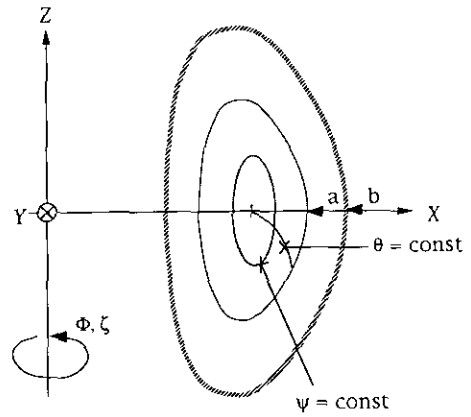

FIG. 1. Flux coordinate system (ψ, θ, ζ). The plasma has a minor radius a. It is surrounded by a vacuum chamber and a conducting wall at distance b from the magnetic axis.

$$q(\psi) \equiv \frac{\mathbf{B}\cdot\nabla\zeta}{\mathbf{B}\cdot\nabla\theta} \tag{2}$$

is a function of the poloidal flux coordinate

$$\psi \equiv \frac{1}{(2\pi)^2}\int d\tau \mathbf{B}\cdot\nabla\theta \tag{3}$$

only. We use ψ as radial coordinate, θ as the poloidal-like coordinate which increases by 2π along the short periodicity length, and ζ as the toroidal-like angle which increases by 2π after one turn in the toroidal direction (see Fig. 1). Note, however, that ζ is not in general equal to the toroidal angle Φ; this happens only when the Jacobian

$$\mathcal{J} \equiv (\nabla\psi \times \nabla\theta \cdot \nabla\zeta)^{-1} \tag{4}$$

of the transformation from (ψ, θ, ζ) to cartesian coordinates (X, Y, Z) is of the form $f(\psi)X^2$. The equilibrium is assumed axisymmetric so that ∂_ζ applied to a scalar quantity is zero.

III. MARGINAL-STABILITY EQUATION FOR THE OUTER REGION

Away from the resonant magnetic surfaces, we are concerned with the solution ξ of the zero-frequency, linearized MHD stability equation [13]

$$\begin{aligned}\mathbf{F}\cdot\boldsymbol{\xi} \equiv & -\mathbf{B}\times[\nabla\times(\mathbf{Q}+\xi_n\mathbf{J}\times\mathbf{n})] \\ & -\mathbf{n}\mathbf{J}\times\mathbf{n}\cdot(\mathbf{Q}+\xi_n\mathbf{J}\times\mathbf{n}) \\ & +2U\nabla\psi\boldsymbol{\xi}\cdot\nabla\psi+\nabla(\Gamma_p\nabla\cdot\boldsymbol{\xi}) = 0.\end{aligned} \tag{5}$$

Here, $\boldsymbol{\xi}$ is the ideal displacement field, $\mathbf{n} \equiv \nabla\psi/|\nabla\psi|$ the unit vector normal to the magnetic surface, $\xi_n \equiv \mathbf{n}\cdot\boldsymbol{\xi}$, $\mathbf{Q} = \nabla\times$

($\boldsymbol{\xi} \times \mathbf{B}$) the magnetic field perturbation, $\Gamma = \frac{5}{3}$ the ratio of specific heats and

$$U \equiv \frac{\mathbf{J} \times \mathbf{n} \cdot (\mathbf{B} \cdot \nabla \mathbf{n})}{|\nabla \psi|^2}. \tag{6}$$

Owing to the assumed continuous symmetry, the ζ dependence of $\boldsymbol{\xi}$ is taken to be that of the single-Fourier mode $\exp(-in\zeta)$, where n is the toroidal-mode number, which we assume to be non-zero. Using (1), this allows one to write

$$\mathcal{J}\mathbf{B} \cdot \nabla \cdot = (\partial_\theta - inq) \cdot \equiv \mathcal{D}_\theta \cdot \tag{7}$$

when applying on a perturbed, scalar quantity.

The parallel displacement is eliminated by the magnetic differential-equation $\mathbf{B} \cdot \nabla(\Gamma p \nabla \cdot \boldsymbol{\xi}) = 0$ obtained when dotting (5) with $\mathbf{B}$, to give the incompressibility condition $\nabla \cdot \boldsymbol{\xi} \equiv 0$ as an exact result [14, 15] for $n \neq 0$. To eliminate the other component of $\boldsymbol{\xi}$ lying within a magnetic surface in favour of the contravariant ψ-component

$$\xi \equiv \boldsymbol{\xi} \cdot \nabla \psi, \tag{8}$$

one dots (5) with $\mathbf{s} \equiv \nabla \psi \times \mathbf{B}/|\nabla \psi|^2$ and obtains [15], again assuming that $n \neq 0$,

$$\mathbf{Q} + \xi_n \mathbf{J} \times \mathbf{n} = \frac{\nabla \psi (\mathbf{B} \cdot \nabla \xi)}{|\nabla \psi|^2} + \nabla_s (\mathcal{G}\mathcal{P}\xi). \tag{9}$$

Here ∇_s is the surface gradient operator $(\mathbf{I} - \mathbf{nn}) \cdot \nabla$, $\mathbf{I}$ being the unit dyadic, $\mathcal{G} \equiv -(\nabla \cdot \nabla_s)^{-1} \mathcal{J}^{-1}$ is the surface Green's function operator, and $\mathcal{P}\xi$ is defined by

$$\mathcal{P}\xi \equiv \mathcal{J} \nabla \cdot \left(\frac{\nabla \psi \mathbf{B} \cdot \nabla \xi - \mathbf{J} \times \nabla \psi \xi}{|\nabla \psi|^2} \right). \tag{10}$$

The $\mathcal{G}$ operator is computed from its inverse

$$\begin{aligned} \mathcal{G}^{-1} = {} & n^2 \mathcal{J} |\nabla_s \zeta|^2 + in(\mathcal{J} \nabla_s \theta \cdot \nabla_s \zeta) \partial_\theta \\ & + \partial_\theta (\mathcal{J} \nabla_s \theta \cdot \nabla_s \zeta) in - \partial_\theta (\mathcal{J} |\nabla_s \theta|^2) \partial_\theta. \end{aligned} \tag{11}$$

Another useful form, which can be obtained from Eqs. (34)–(36) of Dewar, Monticello, and Sy [16], is

$$\begin{aligned} \mathcal{G}^{-1} = {} & -\mathcal{D}_\theta \frac{g(\psi)^2 + |\nabla \psi|^2}{\mathcal{J} B^2 |\nabla \psi|^2} \mathcal{D}_\theta - \mathcal{D}_\theta \frac{g(\psi)}{|\nabla \psi|^2} in \\ & - in \frac{g(\psi)}{|\nabla \psi|^2} \mathcal{D}_\theta + n^2 \mathcal{J} |\mathbf{s}|^2, \end{aligned} \tag{12}$$

with $g(\psi)$ defined as the covariant magnetic field component $\mathbf{B} \cdot \nabla \Phi / |\nabla \Phi|^2$ along the toroidal direction (it can be shown [16] that the ignorability of ζ ensures that g is a function of ψ only).

One can rewrite the operator $\mathcal{P}$ more explicitly,

$$\mathcal{P} = \mathcal{D}_\theta \partial_\psi + \mathcal{Q}, \tag{13}$$

in terms of

$$\begin{aligned} \mathcal{Q} \equiv {} & \mathcal{D}_\theta \frac{\nabla \psi \cdot \nabla \theta}{|\nabla \psi|^2} \mathcal{D}_\theta + \mathcal{D}_\theta \left(\frac{p'}{B^2} - \frac{g\sigma}{|\nabla \psi|^2} + in\mathcal{R} \right) \\ & - in(\mathcal{J}|\mathbf{s}|^2 \sigma + q' + \mathcal{R}_\theta), \end{aligned} \tag{14}$$

where $'$ denotes derivative with respect to ψ,

$$\sigma = \frac{\mathbf{J} \cdot \mathbf{B}}{B^2} = -g' - \frac{gp'}{B^2} \tag{15}$$

measures the parallel current and $\mathcal{R}_\theta \equiv \partial \mathcal{R}/\partial \theta$ the residual shear, with

$$\mathcal{R} \equiv \frac{q \nabla \psi \cdot \nabla \theta - \nabla \psi \cdot \nabla \zeta}{|\nabla \psi|^2} \tag{16}$$

being the integrated residual-shear. The operators ∂_ψ and ∂_θ in (14) act on everything to their right (including the ψ and θ variation in the equilibrium quantities).

Substituting (9) into (5) one obtains the two-dimensional Newcomb equation

$$\mathcal{J} \frac{\nabla \psi \cdot (\mathbf{F} \cdot \boldsymbol{\xi})}{|\nabla \psi|^2} \equiv L\xi = 0, \tag{17}$$

where

$$L\xi = -(\partial_\psi \mathcal{D}_\theta + \mathcal{Q}^\dagger) \mathcal{G} (\mathcal{D}_\theta \partial_\psi + \mathcal{Q}) \xi + \mathcal{K}\xi, \tag{18}$$

and

$$\begin{aligned} \mathcal{K} \equiv {} & 2\mathcal{J}U + \mathcal{J}\mathbf{B} \cdot \nabla \frac{1}{|\nabla \psi|^2} \mathbf{B} \cdot \nabla \\ = {} & 2p' \mathcal{J} \kappa_\psi + \mathcal{J} \sigma^2 |\mathbf{s}|^2 + \sigma(q' + \mathcal{R}_\theta) + \mathcal{D}_\theta \frac{1}{\mathcal{J}|\nabla \psi|^2} \mathcal{D}_\theta. \end{aligned} \tag{19}$$

Here, $\mathcal{K}_\psi \equiv \nabla \psi \cdot (\mathbf{e} \cdot \nabla \mathbf{e})/|\nabla \psi|^2$ is the normal curvature with $\mathbf{e} \equiv \mathbf{B}/B$.

In (18), $\mathcal{Q}^\dagger$ denotes the Hermitian conjugate

$$\langle u, \mathcal{Q}^\dagger v \rangle = \langle \mathcal{Q} u, v \rangle \tag{20}$$

of $\mathcal{Q}$ for arbitrary 2π periodic functions $u(\theta)$ and $v(\theta)$, with

$$\langle u, v\rangle \equiv \int_0^{2\pi} d\zeta \int_0^{2\pi} d\theta\, u^* v = 2\pi \int_0^{2\pi} d\theta\, u^* v \tag{21}$$

defining the surface inner product.

From (11) and (19) we see that $\mathcal{G}$ and $\mathcal{K}$ are Hermitian surface operators

$$\begin{aligned} \mathcal{G}^\dagger &= \mathcal{G} \\ \mathcal{K}^\dagger &= \mathcal{K} \end{aligned} \tag{22}$$

so that

$$(u, Lv) = (Lu, v), \tag{23}$$

where

$$(u, v) \equiv \int_0^{\psi_a} d\psi \langle u, v\rangle \tag{24}$$

for all sufficiently regular u and v, i.e., those belonging to the Hilbert space

$$\mathcal{H} \equiv \{u: |W(u, u)| < \infty\} \tag{25}$$

spanned by all functions for which the ideal energy functional

$$W(u, v) \equiv \tfrac{1}{2}\{(\mathcal{P}u, \mathcal{G}\mathcal{P}v) - (u, \mathcal{K}v) + \langle u, \mathcal{D}_\theta \mathcal{G}\mathcal{P}v\rangle|_{\psi_a}\} \tag{26}$$

is bounded and such that v satisfy natural boundary conditions

$$\mathcal{D}_\theta \mathcal{G}\mathcal{P}v|_{\psi_a} = M(\theta) v(\psi_a, \theta) \tag{27}$$

at the plasma–vacuum interface ψ_a (and regularity condition at $\psi = 0$), $M(\theta)$ being an arbitrary real, 2π-periodic function of θ. The self-adjoint form of L, (18) with (27), ensures that W is symmetric. The reduced ideal stability criterion against global modes [15] then reads

$$W(u, u) > 0 \tag{28}$$

for all non-zero $u \in \mathcal{H}$.

IV. SINGULAR SOLUTIONS

Since $W(\xi, \xi)$ is obtained by integrating $-\frac{1}{2}(\xi, L\xi)$ by parts and keeping the end point contribution, we find the treatment of ideally stable and unstable plasmas for which $W(\xi, \xi) \neq 0$ incompatible with $L\xi = 0$ and $\xi \in \mathcal{H}$. We are therefore led to consider solutions lying outside the Hilbert space $\mathcal{H}$, i.e., solutions which are singular and diverge faster than $x^{-1/2}$. This can occur about the rational surfaces $\psi = \psi_i$, where the safety factor

$$q(\psi_i) = q_i \equiv m_i/n, \tag{29}$$

is rational. The highest order derivative $\partial_\psi \mathcal{D}_\theta \mathcal{G}\mathcal{D}_\theta \partial_\psi$ in (17) has a regular singularity there, as $\partial_\theta - inq$ has a one-dimensional null space spanned by $\exp(im_i\theta)$, with m_i integer. In cylindrical geometry one needs only to consider one rational surface at a time, for a mode with given poloidal m and toroidal n numbers [$\xi \propto \exp i(m\theta - n\zeta)$], provided q is monotonically increasing. However, coupling of the m modes produces in general several coupled rational surfaces in toroidal geometry, for given n. We shall assume the presence of N rational surfaces ψ_i, $0 < \psi_1 < \cdots < \psi_N < \psi_a$ in the plasma, and also assume non-vanishing magnetic shear there, $q'(\psi_i) \neq 0$.

We can then expand all surface operators

$$\begin{aligned} \mathcal{G} &= \mathcal{G}_i + (\psi - \psi_i)\mathcal{G}_i' + (\psi - \psi_i)^2 \mathcal{G}_i''/2 + \cdots \\ \mathcal{Q} &= \mathcal{Q}_i + (\psi - \psi_i)\mathcal{Q}_i' + (\psi - \psi_i)^2 \mathcal{Q}_i''/2 + \cdots \\ \mathcal{K} &= \mathcal{K}_i + (\psi - \psi_i)\mathcal{K}_i' + (\psi - \psi_i)^2 \mathcal{K}_i''/2 + \cdots \\ \mathcal{D}_\theta &= \mathcal{D}_i - (\psi - \psi_i) inq_i' - (\psi - \psi_i)^2 inq_i''/2 + \cdots, \end{aligned} \tag{30}$$

in Taylor series, where $\mathcal{D}_i \equiv \partial_\theta - im_i$, and the solution

$$\begin{aligned} \xi(\psi, \theta) = (\psi - \psi_i)^{\alpha_i} [&\xi_0(\theta) + (\psi - \psi_i)\xi_1(\theta) \\ &+ (\psi - \psi_i)^2 \xi_2(\theta) + \cdots] \end{aligned} \tag{31}$$

in Frobenius series about ψ_i, $i = 1, 2, \ldots, N$. Here, $(\psi - \psi_i)^{\alpha_i}$ has no definite parity so that it should be interpreted as either the even

$$(\psi - \psi_i)_+^{\alpha_i} \equiv |\psi - \psi_i|^{\alpha_i} \tag{32}$$

or the odd

$$(\psi - \psi_i)_-^{\alpha_i} \equiv |\psi - \psi_i|^{\alpha_i} \operatorname{sgn}(\psi - \psi_i) \tag{33}$$

generalized function [17], each parity generating a linearly independent solution which we denote by ξ_+ and ξ_-, respectively. For $\alpha_i = -1, -2, -3, \ldots$, we show, however, in Appendix A that only one parity survives, according to whether α_i is odd or even.

The extraction of the coefficients ξ_k is obtained by inserting (31) and (30) in (17) and equating each order to zero. At lowest order (in $(\psi - \psi_i)^{\alpha_i - 2}$) one finds

$$-(\alpha_i - 1)\mathcal{D}_i \mathcal{G}_i \mathcal{D}_i \alpha_i \xi_0(\theta) = 0, \tag{34}$$

allowing also for the presence of regular solutions having $\alpha_i = 0$ or 1, provided the co-space of $\mathcal{D}_\theta$ is non-empty (i.e., there are non-resonant poloidal modes $m \neq m_i$). The regular solutions, which are locally arbitrary, except for their resonant m_i component, cannot be dismissed in the construction of the global toroidal solution in Section VI; their effect being to

remove the disjointness of the solutions on either side of the singular ψ which exists in the one-dimensional case [11]. However, since their analyticity ensures trivial matching across ψ_i, they are not relevant to the inner layer physics, being merely the extension of the constant Ξ solution of Eq. (21) in GGJ, to the outer region. All toroidal layer models should thus allow for the presence of a displacement solution which is constant (at least at lowest order).

The remaining part of this section therefore deals with the set of singular solutions for which (in general) $\alpha_i \neq 0, 1$, so that from (34) we get

$$\begin{aligned} \mathcal{D}_i \xi_0 &= 0 \\ \mathcal{D}_i \chi_0 &= 0 \end{aligned} \tag{35}$$

purely resonant modes, ξ_0 and $\chi_0 \propto \exp(im_i\theta)$, at lowest order in the Frobenius expansion of ξ, where

$$\chi \equiv \mathcal{G}\mathcal{P}\xi \tag{36}$$

and $\mathcal{D}_\theta \chi$ is, from (9), the total, incompressible, pressure perturbation $\mathbf{B}\cdot\mathbf{Q} - \boldsymbol{\xi}\cdot\nabla p$. It appears therefore more efficient to express (31) as the double Frobenius series [18]

$$\begin{aligned} \mathbf{y}_\pm(\psi,\theta) = (\psi-\psi_i)^{\alpha_i}_\pm \{&\mathbf{y}_0(\theta) + (\psi-\psi_i)\,\mathbf{y}_1(\theta) \\ &+ (\psi-\psi_i)^2 \mathbf{y}_2(\theta) + \cdots\}, \end{aligned} \tag{37}$$

where

$$\mathbf{y} \equiv \begin{pmatrix} \xi \\ \chi \end{pmatrix}, \tag{38}$$

and (17) as the set of first-order equations

$$(\mathbf{A} - \mathbf{I}\mathcal{D}_\theta \partial_\psi)\mathbf{y} = 0 \tag{39}$$

in ψ, where

$$\mathbf{A} \equiv \begin{pmatrix} -\mathcal{Q} & \mathcal{G}^{-1} \\ \mathcal{K} & -(\mathcal{Q} + inq')^\dagger \end{pmatrix}. \tag{40}$$

Writing

$$\mathbf{y}_0 = \mathbf{u}\exp(im_i\theta), \tag{41}$$

we find at next order in the expansion

$$\langle l|\mathbf{y}_1\rangle = \frac{1}{i(l-m_i)(\alpha_i+1)} < l|\mathbf{A}_i|m_i > \mathbf{u}; \quad l \neq m_i, \tag{42}$$

for the non-resonant components (assuming that $\alpha_i \neq -1$), and the eigenvalue problem

$$\langle m_i|\mathbf{A}_i + inq_i'\alpha_i \mathbf{I}|m_i\rangle \mathbf{u} = 0, \tag{43}$$

determining both α_i and $\mathbf{u}$, where

$$\begin{aligned} \langle l|\cdot\rangle &\equiv \frac{1}{2\pi}\int_0^{2\pi} d\theta \exp(-il\theta)\cdot \\ \langle l|\cdot|l'\rangle &\equiv \frac{1}{2\pi}\int_0^{2\pi} d\theta \exp(-il\theta)\cdot\exp(il'\theta) \end{aligned} \tag{44}$$

denote surface averaging (not to be confused with the surface inner product (21)). From (43), one derives the indicial equation

$$(\alpha_i+1)\alpha_i + D_I + \frac{1}{4} = 0 \tag{45}$$

and also a relation between

$$\chi_0 = \frac{\langle m_i|\mathcal{Q}_i|m_i\rangle - inq_i'\alpha_i}{\langle m_i|\mathcal{G}_i^{-1}|m_i\rangle} \tag{46}$$

and the arbitrary coefficient ξ_0, where

$$\begin{aligned} D_I(\psi_i) \equiv &-\frac{1}{4} \\ &+ \frac{\langle m_i|\mathcal{K}_i|m_i\rangle\langle m_i|\mathcal{G}_i^{-1}|m_i\rangle - \langle m_i|\mathcal{Q}_i + inq_i'|m_i\rangle * \langle m_i|\mathcal{Q}_i|m_i\rangle}{n^2 q_i'^2}, \end{aligned} \tag{47}$$

is the Mercier stability index against local ideal modes (again assuming that n and $q_i' \neq 0$). In order for

$$\alpha_i = -\frac{1}{2} \pm \sqrt{-D_I} \tag{48}$$

to be real, we must require that $D_I(\psi_i) < 0$, $i = 1, 2, \ldots, N$. Defining

$$\mu_i \equiv \sqrt{-D_I(\psi_i)}, \tag{49}$$

we obtain the *small solution* $\xi^{(s)}$ by taking $\alpha_i^{(s)} \equiv -\frac{1}{2} + \mu_i$ which can be either positive or negative. The most negative exponent $\alpha_i^{(b)} \equiv -\frac{1}{2} - \mu_i$ in (48) gives rise to a non-square integrable solution $\xi^{(b)}$ ($\alpha^{(b)} < -\frac{1}{2}$) referred to as the *big* (or *large*) *solution*. It is readily seen by introducing (37) into the ideal energy expression (26) that $\xi^{(b)}$ has infinite W, thus $\xi^{(b)} \notin \mathcal{H}$.

Equating order $(\psi-\psi_i)^{\alpha_i+2}$ of (39) to zero, gives

$$\langle l|\mathbf{y}_2\rangle = \frac{1}{i(l-m_i)(\alpha_i+2)} \times \left\{ \sum_{l'} \langle l|\mathbf{A}_i + inq_i'(\alpha_i+1)\,\mathbf{I}\,|l'\rangle \langle l'|\mathbf{y}_1\rangle + \langle l|\mathbf{A}_i'|m_i\rangle\,\mathbf{u} \right\}; \; l \neq m_i, \tag{50}$$

and

$$\langle m_i|\mathbf{y}_1\rangle = -\langle m_i|\mathbf{A}_i + inq_i'(\alpha_i+1)\mathbf{I}|m_i\rangle^{-1} \times \left\{ \sum_{l\neq m_i} \langle m_i|\mathbf{A}_i|l\rangle \langle l|\mathbf{y}_1\rangle + \langle m_i|\mathbf{A}_i' + \tfrac{1}{2}inq_i''\alpha_i\mathbf{I}|m_i\rangle\,\mathbf{u} \right\}. \tag{51}$$

The above procedure to obtain the $\mathbf{y}_k$ can formally be pursued to arbitrary high order assuming that $\alpha_i \neq 0, -1, -2, \ldots$ and no infinite $\mathbf{y}_k$ are encountered on the way. From a numerical viewpoint, however, only the lowest order derivatives of the discretized representations of $\mathfrak{Q}$ etc. can be accurately estimated. This limits to a few orders the maximum number of Frobenius coefficients that can be computed.

V. ZERO-β FROBENIUS EXPANSION

It appears from Eqs. (42) and (50) that Eqs. (31) and (37) cannot be the correct expansions when $\alpha_i = \alpha_i^{(b)} = -1, -2, \ldots$ as this leads to infinite coefficients $\langle l \neq m_i|\xi_k\rangle$. This is not in fact the only circumstance where ξ_k becomes infinite, a similar problem also arises when the matrix $\langle m_i|\mathbf{A}_i + inq_i'(\alpha_i+1)\,\mathbf{I}\,|m_i\rangle$ in (51) is singular which happens when $\alpha_i^{(s)} = \alpha_i^{(b)} + 1$. More generally, the Frobenius coefficients of the big solution diverge at some order if $\mu_i = \frac{1}{2}, 1, \frac{3}{2}, \ldots$. We verify here that the physically important limit of $p'(\psi_i) \to 0$, is one of these "special cases."

From (15) we have $\sigma(\psi_i) \equiv \sigma_i$ independent of θ and using (12), (14), and (19):

$$\langle l|\mathcal{T}_i'|m_i\rangle = -i\sigma_i\langle m_i|\mathfrak{Q}_i|l\rangle^*/n$$
$$\langle l|\mathfrak{Q}_i|m_i\rangle = -inq_i'\delta_{lm_i} - i\sigma_i\langle l|\mathcal{G}_i^{-1}|m_i\rangle/n. \tag{52}$$

Inserting these expressions in (47) we get $D_I = -\frac{1}{4}$ so that

$$\alpha_i^{(s)} = 0, \qquad \alpha_i^{(b)} = -1 \tag{53}$$

take integer values in this limit. Note that the distinction between the regular solution mentioned in Section IV and the continuous component of $\xi^{(s)}$ disappears as both have identical α's. The small solution is thus not uniquely defined; any amount of even $\xi^{(s)}$ can be absorbed into the regular solution, or it can alternatively serve to redefine the big solution whose Frobenius expansion now overlaps the small solution expansion.

Inserting (52) in (43) and (46) we obtain the eigenvectors

$$\mathbf{u}^{(b)} = \begin{pmatrix} 1 \\ -i\sigma_i/n \end{pmatrix}, \qquad \mathbf{u}^{(s)} = \begin{pmatrix} 1 \\ -i\sigma_i/n - inq_i'/\langle m_i|\mathcal{G}_i^{-1}|m_i\rangle \end{pmatrix}, \tag{54}$$

which are used to determine, e.g. (42). Using (52) and (54), it is found that $\langle l|\mathbf{A}_i|m_i\rangle\,\mathbf{u}^{(b)}$ vanishes, thus cancelling the zero in the denominator of (42) so that $\langle l \neq m_i|\mathbf{y}_1^{(b)}\rangle$ yields an arbitrary, *finite contribution which we may set to zero.*

The divergence of the big solution Frobenius coefficients arises at resonant order $\mathcal{O}(|\psi - \psi_i|^{\alpha_i^{(b)}+1})$ here because $\langle m_i|\mathbf{A}_i + inq_i'(\alpha_i^{(b)}+1)\,\mathbf{I}\,|m_i\rangle$ is singular. This is best seen by using the inversion formula

$$\langle m_i|\mathbf{A}_i + inq_i's\,\mathbf{I}\,|m_i\rangle^{-1} = \frac{1}{inq_i'}\left(\frac{\mathbf{u}^{(s)}\overline{\mathbf{u}}^{(s)}}{s+1/2-\mu_i} + \frac{\mathbf{u}^{(b)}\overline{\mathbf{u}}^{(b)}}{s+1/2+\mu_i} \right) \tag{55}$$

that is valid for arbitrary s, with the row vectors

$$\overline{\mathbf{u}}^{(b)} = \langle m_i|\mathcal{G}_i^{-1}|m_i\rangle \quad (i\sigma_i/n + inq_i'/\langle m_i|\mathcal{G}_i^{-1}|m_i\rangle \quad 1)/inq_i'$$
$$\overline{\mathbf{u}}^{(s)} = -\langle m_i|\mathcal{G}_i^{-1}|m_i\rangle \quad (\qquad i\sigma_i/n \qquad 1)/inq_i' \tag{56}$$

being the adjoint eigenvectors, $\overline{\mathbf{u}}\,\langle m_i|\mathbf{A}_i + inq_i'\alpha_i\,\mathbf{I}\,|m_i\rangle = 0$. The eigenvectors and their adjoints satisfy $\overline{\mathbf{u}}^{(b)}\mathbf{u}^{(s)} = \overline{\mathbf{u}}^{(s)}\mathbf{u}^{(b)} = 0$ and $\overline{\mathbf{u}}^{(b)}\mathbf{u}^{(b)} = \overline{\mathbf{u}}^{(s)}\mathbf{u}^{(s)} = 1$. Equations (56) and (54) are *substituted into (51) to yield*

$$\langle m_i|\mathbf{y}_1^{(b)}\rangle = -\frac{\overline{\mathbf{u}}^{(s)}\langle m_i|\mathbf{A}_i'|m_i\rangle\,\mathbf{u}^{(b)}}{inq_i'(1-2\mu_i)}\mathbf{u}^{(s)} - \frac{\overline{\mathbf{u}}^{(b)}[\langle m_i|\mathbf{A}_i'|m_i\rangle - (1/2)inq_i''\,\mathbf{I}]\mathbf{u}^{(b)}}{inq_i'}\mathbf{u}^{(b)}. \tag{57}$$

Thus, $\langle m_i|\mathbf{y}_1^{(b)}\rangle \propto \mathbf{u}^{(s)}$ at leading order in $(1-2\mu_i)^{-1}$; the big solution becomes linearly dependent on the small solution in the limit of $\mu_i \to \frac{1}{2}$, with all but the lowest, resonant order $\mathcal{O}(|\psi - \psi_i|^{\alpha_i^{(b)}})$ and the next non-resonant order $\mathcal{O}(|\psi - \psi_i|^{\alpha_i^{(b)}+1})$ being infinite in (31). It is known [19] that this problem

can be overcome by seeking an independent solution which contains a power expansion times $\ln|\psi - \psi_i|$ in addition to the Frobenius expansion (31). A natural way of motivating this *ansatz* is given in Miller and Dewar [10] and Pletzer and Dewar [18], where a *new big solution*

$$\mathbf{y}_{\pm}^{(b)} \mapsto \mathbf{y}_{\pm}^{(b)} + s_{+}(\mu_i)\mathbf{y}_{\pm}^{(s)} + s_{-}(\mu_i)\mathbf{y}_{\mp}^{(s)} \tag{58}$$

is defined by adding small solution components of same and opposite parities to $\mathbf{y}^{(b)}$. The above equation is of course valid for all μ_i since any linear combination of big and small solutions is also a solution of (39) so that the $s_{\pm}$ are rather arbitrary. When $\langle m_i|\mathbf{y}_k^{(b)}\rangle$ is infinite, however, we take the $s_{\pm}$ corresponding to the appropriate parity (i.e., s_- for $k = 1, 3, \ldots$ and s_{i+} for $k = 2, 4, \ldots$) to cancel the infinite Frobenius term

$$\lim_{\mu_i \to k/2} s(\mu_i) = -\bar{\mathbf{u}}^{(s)}\langle m_i|\mathbf{y}_k^{(b)}\rangle + \mathcal{O}(|k - 2\mu_i|^0), \tag{59}$$

with $\langle m_i|\mathbf{y}_k^{(b)}\rangle \propto \mathbf{u}^{(s)}/(k - 2\mu_i)$, so as to have finite Frobenius coefficients at all orders in the newly defined $\mathbf{y}^{(b)}$. The well-known logarithmic terms in the expansion arise here naturally after taking the limit,

$$\lim_{\mu_i \to k/2} \frac{(\psi - \psi_i)^{-1/2-\mu_i+k} - (\psi - \psi_i)^{-1/2+\mu_i}}{k - 2\mu_i} = (\psi - \psi_i)^{-1/2+\mu_i}\ln|\psi - \psi_i|. \tag{60}$$

As we have $\alpha^{(s)} = \alpha^{(b)} + 1$ at $\beta = 0$, we choose

$$s_{-}(\tfrac{1}{2}) = \frac{\bar{\mathbf{u}}^{(s)}\langle m_i|\mathbf{A}_i'|m_i\rangle\,\mathbf{u}^{(b)}}{inq_i'(1 - 2\mu_i)} \tag{61}$$

in (59), to find the new big solution

$$\begin{aligned}\mathbf{y}_{\pm}^{(b)} \mapsto \mathbf{y}_{\pm}^{(b)} = {} & \frac{\mathbf{u}^{(b)}}{\psi - \psi_i}\exp(im_i\theta) \\ & - \frac{\bar{\mathbf{u}}^{(s)}\langle m_i|\mathbf{A}_i'|m_i\rangle\,\mathbf{u}^{(b)}}{inq_i'}\mathbf{u}^{(s)}\ln|\psi - \psi_i|\exp(im_i\theta) \\ & - \frac{\bar{\mathbf{u}}^{(b)}[\langle m_i|\mathbf{A}_i'|m_i\rangle - \mathbf{I}\,inq_i''/2]\mathbf{u}^{(b)}}{inq_i'}\mathbf{u}^{(b)}\exp(im_i\theta) \\ & + \mathcal{O}(|\psi - \psi_i|\ln|\psi - \psi_i|) + \mathcal{O}(\psi - \psi_i)\end{aligned} \tag{62}$$

which is (purely) resonant up to $\mathcal{O}(|\psi - \psi_i|^0)$. In the following, we assume that we are dealing with big solutions that are properly defined for all values of μ_i (no infinite Frobenius coefficients); hence we will implicitly assume the renormalization (58) for half-integer values of μ_i. It has been customary to take $s(\mu_i) = 0$ in most preceding works [5]; this is only appropriate for $2\mu_i \neq k$. Taking $s(\mu_i) \neq 0$ for other values of μ_i is permitted provided the inner solutions undergo the same renormalization so that the matching between outer and inner solutions remains consistent. This point will further be discussed in Section VIII.

VI. GLOBAL SOLUTION EXPANSION

In order to construct the most general outer solution, let us focus on a rational surface ψ_i in which vicinity we write the solution of the outer equation (17) as

$$\xi = \sum_p \{\xi_p^{(b)}c_{ip}^{(b)} + \xi^{(s)}c_{ip}^{(s)}\} + \mathcal{O}(\xi^{(r)}), \quad \psi_i - R_i < \psi < \psi_i + R_i, \tag{63}$$

a linear combination of big and small Frobenius solutions of even $p = +$ and odd $p = -$ parity, plus a regular solution $\mathcal{O}(\xi^{(r)})$. Equation (63) is valid within the radius of convergence R_i of the Frobenius expansions. In the "special case," where $\alpha_i^{(b)}$ is an integer, the regular solution can be adsorbed in the big solution and the sum in (63) involves only one parity (e.g., $p = -$ for $\alpha_i^{(b)} = -1$).

Due to the linearity of the outer equation, the only relevant data for the matching of outer to inner solutions are the ratios of small coefficients $c_{i\pm}^{(s)}$ to big coefficients $c_{i\pm}^{(b)}$, which must be evaluated at all rational surfaces $i = 1, 2, \ldots, N$. These coefficients depend on Eq. (17) and on the boundary conditions (27). They can be computed assuming, e.g., the $c^{(b)}$'s to be held fixed so that the $c^{(s)}$'s may be regarded as response coefficients to driven big solutions. (The converse where the $c^{(b)}$'s are determined in relation to the $c^{(s)}$'s can also be done [8] but is numerically more tricky, the big solutions being strongly singular.) In the present approach, we choose to prescribe the big solutions *via* their Frobenius expansion, whereas the small (and regular) solutions are determined numerically. However, since it is, in practice, impossible to compute the infinite number of terms in (31), we must be content with prescribed solutions that approximate the exact $\xi^{(b)}$ to sufficient order.

Let $\hat{\xi}_{ip}$ be the *prescribed solution* which possesses the big solution behaviour of parity p as $\psi \to \psi_i$ and ξ_{ip} be a *fundamental solution* of (17), we define the *response solution* $\check{\xi}_{(ip)}$ satisfying the forced equation

$$L\check{\xi}_{(ip)} = -L\hat{\xi}_{ip} \tag{64}$$

for all $i = 1, 2, \ldots, N$ and relevant parities p, as

$$\check{\xi}_{(ip)} \equiv \xi_{ip} - \hat{\xi}_{ip}. \tag{65}$$

The condition that $\hat{\xi} \sim \xi^{(b)}$ to sufficient accuracy is

$$\check{\xi}_{(ip)} \in \mathcal{H}; \tag{66}$$

i.e., $\check{\xi}$ must be square integrable, therefore involving only small and regular solution components to leading order. To satisfy (66), we require the source term in (65)

$$L\hat{\xi}_{ip} = o(\xi^{(s)}) \quad \text{as } \psi \to \psi_i \tag{67}$$

to be of order recessive to $\xi^{(s)}$; that is, the effect of L on $\hat{\xi}$ is to annihilate each term in the big Frobenius expansion up to an order $(\psi - \psi_i)^{\alpha_i^{(b)}+k}$ which vanishes faster than the small solution. Here, $k-1$ represents the order at which the expansion of $\hat{\xi}$ can be truncated so as to have

$$\lim_{\psi \to \psi_i} (\hat{\xi}_{ip} - \xi_p^{(b)}) = o(\xi^{(s)}). \tag{68}$$

The truncation order is in general different for the resonant $l = m_i$ and non-resonant $l \neq m_i$ poloidal modes. The following table gives the minimum number N_r of resonant and N_n of non-resonant Frobenius terms $\langle l|\xi_k^{(b)}\rangle$ to include in $\hat{\xi}$ for various μ_i:

	$0 < \mu_i < \frac{1}{2}$	$\mu_i = \frac{1}{2}$	$\frac{1}{2} < \mu_i < 1$	$\cdots$
N_r:	1	2 + log	2	$\cdots$
N_n:	1	0	2	$\cdots$

(69)

In the $\beta = 0$ case, the mixed Frobenius and logarithmic expansion involves the resonant terms expounded in (62).

Conditions (68) and (67) are satisfied by

$$\hat{\xi}_{ip} = \frac{\xi_p^{(b)}}{2\mu_i f_i} + o(\xi^{(s)}) \quad \text{as } \psi \to \psi_i, \tag{70}$$

where $o(\xi^{(s)})$ represents the truncation error of the big expansion and

$$f_i \equiv \frac{4\pi^2 n^2 q_i'^2}{\langle m_i|\mathcal{G}_i^{-1}|m_i\rangle}, \tag{71}$$

a positive normalization factor which will turn out to be convenient.

Although $\hat{\xi} \notin \mathcal{H}$, we wish to have similar Hermiticity properties to those (23) satisfied by square-integrable displacements. This requires $\hat{\xi}_{ip}$ to be "well behaved" (e.g., of $\mathbb{O}(\xi^{(s)})$) at all $\psi_j \neq \psi_i$, $j = 1, 2, \ldots, N$. As the behaviour of $\hat{\xi}_{ip}$ is otherwise arbitrary away from ψ_i, we find it convenient to limit the support of $\hat{\xi}_{ip}$ by multiplying it with the bell-shaped function shown in Fig. 2, whose extension is shorter than the distance separating ψ_i to the nearest rational surface, respectively $\psi = 0$ for $i = 1$ or ψ_a for $i = N$. That is,

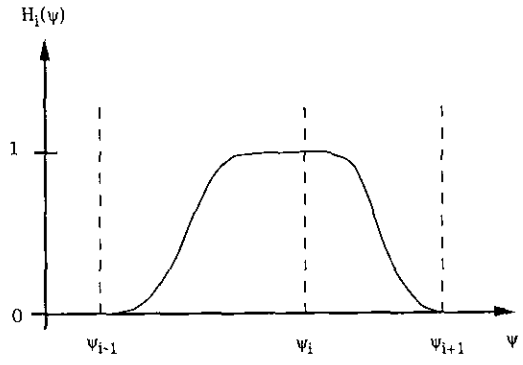

FIG. 2. The bell-shaped functions H_i which are approximately flat about ψ_i and whose support does not overlap the neighbouring rational surfaces.

$$\hat{\xi}_{ip}(\psi_j) \equiv 0, \quad j \neq i, \tag{72}$$

and

$$\left.\begin{aligned} \hat{\xi}_{ip}(\psi = 0) \\ \hat{\xi}_{ip}(\psi = \psi_a) \end{aligned}\right\} \equiv 0. \tag{73}$$

Applying this prescription to all rational surfaces we then write the most general solution

$$\xi = \sum_p \sum_{i=1}^{N} \xi_{ip} c_{ip} \tag{74}$$

as an expansion, $c_{ip} = 2\mu_i f_i c_{ip}^{(b)}$, in fundamental solutions $\xi_{ip} = \check{\xi}_{(ip)} + \hat{\xi}_{ip}$, with $\check{\xi}_{(ip)}$ extracted using (64) and $\hat{\xi}_{ip}$ prescribed by (70).

VII. DISPERSION RELATION

Using assumption (66), we seek a weak solution

$$W(u, \check{\xi}_{(ip)}) = \tfrac{1}{2}(u, L\hat{\xi}_{ip}), \tag{75}$$

where W is defined by (26). Equation (75) is obtained by multiplying (64) by an arbitrary test function $u \in \mathcal{H}$ and integrating the left-hand side by parts. It is readily seen that the boundedness of W: $|W(u, \check{\xi}_{(ip)})| < \infty \ \forall u$ such that $(u, u) < \infty$ combined with (67) guarantee that

$$\check{\xi}_{(ip)} = \sum_{q=+,-} \xi_q^{(s)} D'_{jq,ip} + o(\xi^{(s)}) + \mathbb{O}(\xi^{(r)}) \quad \text{as } \psi \to \psi_j, \tag{76}$$

$j = 1, 2, \cdots, N$, is depleted of $\xi^{(b)}$'s. Note that $\check{\xi}_{(ip)}$ extends

over the entire plasma and exhibits a mixture of even and odd asymptotic parities, even though $\hat{\xi}_{ip}$ is localized and has definite parity. (In cylindrical geometry, the absence of regular solution prevents the response solution to "leak" across the rational surfaces, confining $\check{\xi}_{(ip)}$ to within (ψ_{i-1}, ψ_{i+1}).) The brackets around the indices ip are therefore a reminder that these refer to the localization/parity of the driving $\hat{\xi}$.

The proportionality coefficients $D'_{jq,ip}$ between $\check{\xi}$ and $\xi^{(s)}$ form the *outer matching matrix*

$$\mathbf{D}' \equiv \tfrac{1}{2}\begin{bmatrix} \mathbf{A}' & \mathbf{B}' \\ \Gamma' & \mathbf{\Delta}' \end{bmatrix}, \tag{77}$$

which contains $N \times N$ submatrices $\frac{1}{2}\mathbf{A}' \equiv \frac{1}{2}(A'_{ji}) = D'_{j+,i+}$ etc., representing the even and odd small solution response coefficients,

$$c^{(s)}_{jq} \equiv \sum_{ip} D'_{jq,ip} c_{ip} = 2 \sum_{ip} D'_{jq,ip} \mu_i f_i c^{(b)}_{ip}, \tag{78}$$

to driving big solution of even and odd parity, respectively. The matching matrix $\mathbf{D}'$ forms a complete set of data allowing for the matching of outer to inner solutions, regardless of the inner layer model.

We use capital letters to denote the Frobenius solutions

$$\Xi^{(b,s)}_p = \left(\frac{\psi - \psi_i}{L_i}\right)^{\alpha_i^{(b,s)}}_p + \mathcal{O}\left(\left|\frac{\psi - \psi_i}{L_i}\right|^{\alpha_i^{(b,s)}-1}\right) \quad \text{as } \frac{\psi - \psi_i}{L_i} \to \pm\infty \tag{79}$$

arising in the inner layers i, $i = 1, 2, \ldots, N$, of width $L_i \to 0$. Similarly, we write the inner fundamental solutions as

$$\Xi_{ip} = \sum_q \left\{ \frac{\Xi^{(b)}_q \delta_{ji}\delta_{qp}}{2\mu_j f_j} + \Xi^{(s)}_q L^{\alpha^{(s)}_j} D_{jq,ip}(\gamma) L^{-\alpha^{(b)}_i} \right\} \quad \text{as } (\psi - \psi_j)/L_j \to \pm\infty \tag{80}$$

and the global solution as

$$\Xi = \sum_{ip} \Xi_{ip} C_{ip}. \tag{81}$$

Equations (79)–(81) are defined by analogy to Eqs. (74), (70), and (76). The condition that the outer solution (74) match the inner solution in the region of overlap, i.e., where $\psi \to \psi_j$ and $(\psi - \psi_j)/L_j \to \pm\infty$, yields

$$C_{ip} = L^{\alpha^{(b)}_i} c_{ip} \tag{82}$$

and

$$\mathbf{D}'\mathbf{c} = \mathbf{D}(\gamma)\mathbf{c}, \tag{83}$$

where $\mathbf{c}^{\mathsf{T}} = (c_{1+} \cdots c_{N+}\, c_{1-} \cdots c_{N-})$ is the vector of coefficients c_{ip} in (74), leading to the dispersion relation

$$\det[\mathbf{D}' - \mathbf{D}(\gamma)] = 0 \tag{84}$$

for the growth rate γ, with the matching matrices $\mathbf{D}'$ and $\mathbf{D}(\gamma)$ obtained by solving the outer and, inner equations, respectively. Expression (84) applies to general asymmetric (with respect to the ψ_i) layers for which the inner matching data matrix $\mathbf{D}(\gamma)$ is full [8]. In the analytical inner layer model of GGJ [5], the inner solutions of complementary parity and those located in different layers ψ_i decouple so that

$$\mathbf{D}(\gamma) = \tfrac{1}{2}\begin{bmatrix} (A_i(\gamma)\delta_{ij}) & (0) \\ (0) & (\Delta_i(\gamma)\delta_{ij}) \end{bmatrix} \tag{85}$$

becomes diagonal, with the inner data being related

$$\begin{aligned} A_i &\equiv \Delta_{i+}/\mu_i f_i L_i^{2\mu_i} \\ \Delta_i &\equiv \Delta_{i-}/\mu_i f_i L_i^{2\mu_i} \end{aligned} \tag{86}$$

to the inner matching data $\Delta_\pm$ of Ref. [20].

From the discussion in Section V, only the $\mathbf{\Delta}'$ submatrix is relevant in the pressureless limit, simplifying (84) even further to the *tearing mode dispersion relation*

$$\det\left(\Delta'_{ji} - \frac{\Delta_{i-}(\gamma)\delta_{ji}}{\mu_i f_i L_i^{2\mu_i}}\right) = 0. \tag{87}$$

VIII. EXTRACTION OF THE OUTER MATCHING DATA

The outer matching data (77) are the leading coefficients of the small Frobenius solution present in $\check{\xi}$. In the cases where $\xi^{(r)}$ is recessive to $\xi^{(s)}$ in (76), as in cylindrical geometry or when $\mu < \frac{1}{2}$ in toroidal geometry there exists a simple formula

$$D'_{jq,ip} = \lim_{\psi \to \psi_i} \check{\xi}_{(ip)}/(\psi - \psi_j)^{\alpha^{(s)}_q}_j, \quad \mu_j < \tfrac{1}{2}, \tag{88}$$

based on the asymptotic behaviour of $\check{\xi}_{(ip)}$ about ψ_j.

Since $\xi^{(r)}$ may be absorbed into $\xi^{(b)}$ in the $\beta = 0$ case, the regular solution can be dismissed so that (88) applies there also. Recalling that only the odd parity $\hat{\xi}$ is selected when $\beta = 0$ and that only the discontinuous part of $\check{\xi}$ matters, (88) then reduces to

$$\Delta' = [\![\check{\xi}_{(i-)}]\!]_i, \quad \mu_i = \tfrac{1}{2}, \tag{89}$$

the jump,

$$[\![\cdot]\!]_j \equiv \lim_{\epsilon\to 0+} \{[\cdot]_{\psi_j+\epsilon} - [\cdot]_{\psi_j-\epsilon}\}, \tag{90}$$

of $\check{\xi}_{(i-)}$ across ψ_j. This expression is equivalent to the definition $\Delta' = [\![\partial_\psi(\mathbf{B}\cdot\nabla\xi)/\mathbf{B}\cdot\nabla\xi]\!]$ dating back to Furth, Killeen, and Rosenbluth [4].

Seeking a formula for $\mathbf{D}'$ valid for all μ's in toroidal geometry, we introduce the surface bilinear concomitant [21]

$$P(u, v|\psi) = -\langle u, \mathcal{D}_\theta \mathcal{GP} v\rangle + \langle \mathcal{D}_\theta \mathcal{GP} u, v\rangle \tag{91}$$

with $\langle\cdot,\cdot\rangle$ defined in (21), which arises from

$$\langle u, Lv\rangle = \partial_\psi P(u, v|\psi) + \langle Lu, v\rangle, \quad u, v \in \mathcal{H}, \tag{92}$$

when performing double integration by parts on L. We emphasize here that (92) is valid only if u and v are reasonably "well behaved" functions. The bilinear concomitant is sometimes used to extract a linearly independent solution from a differential equation. It may be thought of as a generalized Wronskian. Taking $u = \xi^{(b)}$ and v as either the small or the regular solution, we immediately see from (92) that $P(\xi^{(b)}, \xi^{(i)}|\psi)$ is pointwise constant *except* at the rational surfaces (where $\xi^{(b)}$ is badly behaved).

We shall first evaluate this constant for $u = \xi_p^{(b)}$ and $v = \xi_q^{(s)}$. This is straightforward as we have already derived the Frobenius expansion of $\chi = \mathcal{GP}\xi = (\psi - \psi_i)^\alpha \{\chi_0 + \chi_1(\psi - \psi_i) + \cdots\}$ in Section IV. Using a similar expansion for $P(\xi_p^{(b)}, \xi_q^{(s)}) = (\psi - \psi_i)^{\alpha_{qp}^{(b)} + \alpha^{(s)}} \{P_0 + P_1(\psi - \psi_i) + \cdots\}$, we obtain $P_0 = 0$ since ξ_0 and χ_0 are purely resonant and $P_1 = 2\mu_i f_i$ after taking $\xi_0^{(b)} = \xi_0^{(s)} = 1$, using (46) and noting the anti-Hermitian property $\langle m_i|\mathcal{Q}_i|m_i\rangle^* = -\langle m_i|\mathcal{Q}_i|m_i\rangle$ following from (14), with f_i defined in (71). One can show that all higher order terms P_k, $k \geq 2$, vanish. We are thus left with

$$P(\xi_p^{(b)}, \xi_q^{(s)}) = 2\mu_i f_i (\psi - \psi_i)^0_{-pq}, \tag{93}$$

so that, according to our notation where $x_+^0 \equiv 1$ and $x_-^0 \equiv \operatorname{sgn} x$, $P(\xi^{(b)}, \xi^{(s)})$ is *discontinuous*,

$$[\![P(\xi_p^{(b)}, \xi_q^{(s)})]\!]_i = 4\mu_i f_i \delta_{pq}, \tag{94}$$

at ψ_i if $\xi^{(b)}$ and $\xi^{(s)}$ have the *same parity*. We now see that to make (92) true in a generalized function sense, we must subtract off the δ function contributions at the rational surfaces, yielding an equation that is reminiscent of that defining a Green's function,

$$\langle u, Lv\rangle = \partial_\psi P(u, v|\psi) - \sum_i [\![P(u, v)]\!]_i \delta(\psi - \psi_i) + \langle Lu, v\rangle. \tag{95}$$

The Hermiticity condition $(u, Lv) = (Lu, v)$ then only holds if u and v satisfy the physical boundary conditions (27) and if $[\![P(u, v)]\!]_i = 0$ at all ψ_i.

Focusing on $P(\xi^{(b)}, \xi^{(r)})$ we find that the assumption of constant P is incompatible with the power series representation $(\psi - \psi_i)^{\alpha^{(b)}} \{P_0 + P_1(\psi - \psi_i) + \cdots\}$ for all non-integer $\alpha^{(b)}$, unless all the coefficients P_k vanish so that

$$[\![P(\xi^{(b)}, \xi^{(r)})]\!]_i = 0. \tag{96}$$

This can be verified [22] explicitly to hold for $\mu \neq \frac{1}{2}, 1, \frac{3}{2}, \ldots$. The concomitant between the big and the regular solution must hence be zero everywhere except when μ is a half integer.

We therefore get from (95),

$$\tfrac{1}{2}(\hat{\xi}_{ip}, L\check{\xi}_{(jq)}) = \tfrac{1}{2}(L\hat{\xi}_{ip}, \check{\xi}_{(jq)}) - \tfrac{1}{2}[\![P(\hat{\xi}_{ip}, \check{\xi}_{(jq)})]\!]_i, \tag{97}$$

after recalling that the $\hat{\xi}$ have supports vanishing at the boundaries (73). Inserting (96) and (93) in (76), we find

$$\tfrac{1}{2}[\![P(\hat{\xi}_{ip}, \check{\xi}_{(jq)})]\!]_i = D'_{ip,jq}, \tag{98}$$

so that (95) reduces to the fundamental result

$$D'_{ip,jq} = W(\check{\xi}_{(ip)}, \check{\xi}_{(jq)}) + \tfrac{1}{2}(\hat{\xi}_{ip}, L\hat{\xi}_{jq}), \tag{99}$$

which expresses the outer matching data matrix in terms of the ideal energy functional W involving the response solutions (65) and a "prescribed energy" composed of the predetermined $\hat{\xi}$ only. This is referred to as the GGF method, as $\hat{\xi}$ and $\check{\xi}$ play a similar role in (97) to that of a solution and its Green's function.

A number of interesting properties are immediately apparent from (99). Since $(\hat{\xi}_{ip}, L\hat{\xi}_{jq})$ is symmetric under the interchange of ip and jq by virtue of the localization hypothesis (72) and (73) of $\hat{\xi}$, we also have

$$D'_{ip,jq} = D'^{\dagger}_{jq,ip}. \tag{100}$$

It was shown in [11] that this property is intimately related to the existence of a variational principle: $\delta D'_{ip,jq}/\delta\check{\xi}^*_{(ip)} = \delta D'_{ip,jq}/\delta\check{\xi}_{(jq)} = 0$ for $\check{\xi}_{(ip)}$ and $\check{\xi}_{(jq)}$ satisfying (64).

Most plasmas being characterized by small β values such that $\alpha^{(s)}$ and $\alpha^{(b)}$ are nearly integers, it is therefore of interest to study the impact of renormalizing the big solution

$$\left.\begin{aligned}\hat{\xi}_{jq} &\mapsto \hat{\xi}_{jq} + s_{j+}\xi_q^{(s)} + s_{j-}\xi_{-q}^{(s)}\\ \check{\xi}_{(jq)} &\mapsto \check{\xi}_{(jq)} - s_{j+}\xi_q^{(s)} - s_{j-}\xi_{-q}^{(s)}\end{aligned}\right\} \quad \text{as } \psi \to \psi_j \tag{101}$$

on the determination of the matching matrix $\mathbf{D}'$. Transformation (101) is similar to (58), satisfying (67) while keeping $\xi_{jq} = \check{\xi}_{(jq)} + \hat{\xi}_{jq}$ invariant. We assume here that the transformation takes place at ψ_j only, so that $\hat{\xi}_{jq}$ remains localized in agreement

with prescriptions (72) and (73). Using Eqs. (98) and (94) we obtain

$$D'_{ip,jq} \mapsto \tilde{D}'_{ip,jq} \equiv D'_{ip,jq} - \delta_{ij}(\delta_{pq}s_{j+} + \delta_{p,-q}s_{j-}), \quad (102)$$

which shows, in particular, that $s_{j-} \neq 0$ leaves the submatrices $\mathbf{A}'$ and $\mathbf{\Delta}'$ unaffected, their limit as $\beta \to 0$ remaining well defined. Here, we distinguish the matching data $D'_{jq,ip}$ from the transformed matching data $\tilde{D}'_{jq,ip}$ which do not, strictly speaking, represent the coefficients of small to big solutions. To remain consistent with the usual approach [4, 5], we will perform the matching using the untransformed matrix $\mathbf{D}'$ in Section XI.

Finally, let us point out that the ideal stability criterion (28) is contained in (99) [23] as $D'_{ip,jq}$ has the same definiteness as W near the marginal stability point where the prescribed contribution to the energy becomes negligible with respect to the ideal part. A clear manifestation of a transition from ideal stability to instability thus translates into a sharp drop from $+\infty$ to $-\infty$ in the behaviour of the eigenvalues of $D'_{ip,jq}$.

IX. IMPLEMENTATION OF THE GGF SCHEME

If we multiply the response equations (65) by an arbitrary, well-behaved function $-\frac{1}{2}u^*$ and integrate over the plasma, we find

$$W(u, \check{\xi}_{(ip)}) = \tfrac{1}{2}(u, L\hat{\xi}_{ip}). \quad (103)$$

Equation (103) is called the *weak form* of (64). But rather than computing $L\hat{\xi}$ by taking the truncated Frobenius expansion of $\xi^{(b)}$ and applying the L operator on it, we prefer to make use of the double expansion (37) by adding two (cancelling) terms involving $\hat{\chi}_{ip}$,

$$\begin{aligned} L\hat{\xi}_{ip} = &-(\partial_\psi \mathcal{D}_\theta + \mathcal{Q}^\dagger)\hat{\chi}_{ip} + \mathcal{K}\hat{\xi}_{ip} \\ &+ (\partial_\psi \mathcal{D}_\theta + \mathcal{Q}^\dagger)(\hat{\chi}_{ip} - \mathcal{G}\mathcal{P}\hat{\xi}_{ip}), \end{aligned} \quad (104)$$

in the source term. This is motivated by the observation that if $\hat{\xi}_{ip}$ is rather arbitrary away from the rational surfaces, so is the conjugate variable $\hat{\chi}_{ip}$ which can depart from $\mathcal{G}\mathcal{P}\hat{\xi}_{ip}$ as long as

$$\left.\begin{aligned} \hat{\chi}_{ip} - \mathcal{G}\mathcal{P}\hat{\xi}_{ip} &\sim o(\xi^{(s)}) \\ -(\partial_\psi \mathcal{D}_\theta + \mathcal{Q}^\dagger)\hat{\chi}_{ip} + \mathcal{K}\hat{\xi}_{ip} &\sim o(\xi^{(s)}) \end{aligned}\right\} \quad \text{as } \psi \to \psi_i \quad (105)$$

by analogy to (67). Thus, the discrepancy between $\hat{\chi}$ and $\mathcal{G}\mathcal{P}\hat{\xi}$ must be of the same order as the correction (68) between $\hat{\xi}$ and $\xi^{(b)}$. Inserting (104) in (103) and integrating by parts the term $(u, \partial_\psi \mathcal{D}_\theta[\hat{\chi} - \mathcal{G}\mathcal{P}\hat{\xi}])$—permitted as $(\hat{\chi} - \mathcal{G}\mathcal{P}\hat{\xi}) \in \mathcal{H}$—we obtain the new weak form,

$$\begin{aligned} W(u, \check{\xi}_{(ip)}) = &\tfrac{1}{2}(u, -[\partial_\psi \mathcal{D}_\theta + \mathcal{Q}^\dagger]\hat{\chi}_{ip} + \mathcal{K}\hat{\xi}_{ip}) \\ &+ \tfrac{1}{2}(\mathcal{P}u, \hat{\chi}_{ip} - \mathcal{G}\mathcal{P}\hat{\xi}_{ip}), \end{aligned} \quad (106)$$

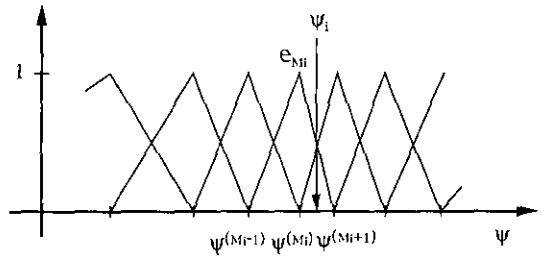

FIG. 3. Nonuniform distribution of radial basis functions e_k about a rational surface ψ_i, whose position is indicated by the vertical arrow. Each element e_k extends from node $\psi^{(k-1)}$ to node $\psi^{(k+1)}$. There are M_i finite elements in $(0, \psi_i)$. The two adjacent elements $k = M_i$ and $k = M_i + 1$ are equidistant from ψ_i.

which, while being equivalent to (103), possesses some important numerical advantages. In particular, only first-order ∂_ψ operators are present in (106), compared to second order in (103). Second, no derivatives of $\mathcal{G}$ and $\mathcal{Q}$ need to be computed, except at the rational surfaces for the determination of the Frobenius expansion. This results in an increase in accuracy which has a particularly beneficial effect when $\alpha^{(s)}$ and $\alpha^{(b)}$ differ by a large amount, so that many Frobenius terms are required in $\hat{\xi}$ in order for L to kill (approximately) the singularity in (67). The use of expression (104) is not limited to the weak form only, multiplying (104) by $\frac{1}{2}\hat{\xi}^*_{jq}$ and using condition (105) such that $(\hat{\xi}_{jq}, [\partial_\psi \mathcal{D}_\theta + \mathcal{Q}^\dagger]o(\xi^{(s)}))$ can be freely integrated by parts, we find the quasi-Hamiltonian form of the prescribed energy,

$$\begin{aligned} \tfrac{1}{2}(\hat{\xi}_{jq}, L\hat{\xi}_{ip}) = &\tfrac{1}{2}(\hat{\xi}_{jq}, -[\partial_\psi \mathcal{D}_\theta + \mathcal{Q}^\dagger]\hat{\chi}_{ip} + \mathcal{K}\hat{\xi}_{ip}) \\ &+ \tfrac{1}{2}(\mathcal{P}\hat{\xi}_{jq}, \hat{\chi}_{ip} - \mathcal{G}\mathcal{P}\hat{\xi}_{ip}), \end{aligned} \quad (107)$$

used in (99) to determine the outer matching data.

We approximate the solution $\check{\xi}_{(ip)}$ by the finite expansion (Ritz approximation)

$$\check{\xi}^{(M)}_{(ip)} = \sum_{k=1}^{M} \sum_{l=L}^{L} \Xi^{(k,l)}_{ip} e^{(l)}_k(\psi, \theta) \quad (108)$$

in the basis functions

$$e^{(l)}_k(\psi, \theta) \equiv e_k(\psi)\exp(il\theta) \quad (109)$$

with $e_k(\psi)$ belonging to the Sobolev space $\mathcal{H}_M$ and $\exp(il\theta)$ spanning the finite-dimensional Fourier space $\mathcal{H}_{L,L}$: $\check{\xi}^{(M)}_{(ip)} \in \mathcal{H}_M \otimes \mathcal{H}_{L,L} \subset \mathcal{H}$. A typical choice of finite elements $e_k(x)$ is shown in Fig. 3: these are the linear tent-functions which are non-zero between $\psi^{(k-1)}$ and $\psi^{(k+1)}$ (except for e_1 and e_M which have supports extending from $\psi^{(1)} = 0$ to $\psi^{(2)}$ and $\psi^{(M-1)}$ to $\psi^{(M)} = \psi_a$, respectively).

Replacing $\check{\xi}_{(ip)}$ by $\check{\xi}^{(M)}_{(ip)}$ in (106), we find the set of $M \times (\hat{L} - \check{L} + 1)$ *Galerkin equations*

$$W(u, \check{\xi}^{(M)}_{(ip)}) = \tfrac{1}{2}(u, -[\partial_\psi \mathcal{D}_\theta + \mathcal{Q}^\dagger]\hat{\chi}_{ip} + \mathcal{K}\hat{\xi}_{ip}) + \tfrac{1}{2}(\mathcal{P}u, \hat{\chi}_{ip} - \mathcal{G}\mathcal{P}\hat{\xi}_{ip}), \tag{110}$$

which leads, after substituting (108) into (110) and setting $u = e^{(l')}_{k'}$, to the system of linear equations

$$\sum_{k=1}^{M}\sum_{l=\check{L}}^{\hat{L}} W(e^{(l')}_{k'}, e^{(l)}_{k})\Xi^{(k,l)}_{ip} = \tfrac{1}{2}(e^{(l')}_{k'}, -[\partial_\psi \mathcal{D}_\theta + \mathcal{Q}^\dagger]\hat{\chi}_{ip} + \mathcal{K}\hat{\xi}_{ip}) + \tfrac{1}{2}(\mathcal{P}e^{(l')}_{k'}, \hat{\chi}_{ip} - \mathcal{G}\mathcal{P}\hat{\xi}_{ip}), \tag{111}$$

for the coefficients $\Xi^{(k,l)}_{ip}$. Equations (111) admit a unique solution, provided the integral on the right-hand side converges.

The estimate $\mathbf{D}'^{(M)}$ for the matching data $\mathbf{D}'$ is obtained by replacing $\check{\xi}$ by their respective finite-element expansions $\check{\xi}^{(M)}$, giving

$$D'^{(M)}_{jq,ip} = \sum_{k,k'}\sum_{l,l'} \Xi^{(k',l')}_{jq} * W(e^{(l')}_{k'}, e^{(l)}_{k})\Xi^{(k,l)}_{ip} + \tfrac{1}{2}(\hat{\xi}_{jq}, -[\partial_\psi \mathcal{D}_\theta + \mathcal{Q}^\dagger]\hat{\chi}_{ip} + \mathcal{K}\hat{\xi}_{ip}) + \tfrac{1}{2}(\mathcal{P}\hat{\xi}_{jq}, \hat{\chi}_{ip} - \mathcal{G}\mathcal{P}\hat{\xi}_{ip}). \tag{112}$$

X. FINITE ELEMENT CONVERGENCE AND MESH GENERATION

Choosing $u \in \mathcal{H}_M \otimes \mathcal{H}_{\check{L}\hat{L}}$ in the weak form (106) and subtracting (110) from it, it is seen,

$$W(u, \check{\xi}_{(ip)} - \check{\xi}^{(M)}_{(ip)}) = 0, \tag{113}$$

that the error $\varepsilon_{ip} \equiv \check{\xi}_{(ip)} - \check{\xi}^{(M)}_{(ip)}$ is *orthogonal*, with respect to the energy inner-product, to any function belonging to $\mathcal{H}_M \otimes \mathcal{H}_{\check{L}\hat{L}}$. The error resulting from approximating the matching data $\mathbf{D}'$ by $\mathbf{D}'^{(M)}$,

$$D'_{jq,ip} - D'^{(M)}_{jq,ip} = W(\check{\xi}_{(jq)}, \check{\xi}_{(ip)}) - W(\check{\xi}^{(M)}_{(jq)}, \check{\xi}^{(M)}_{(ip)}) = W(\varepsilon_{jq}, \varepsilon_{ip}), \tag{114}$$

is thus proportional to the square of the energy norm, a characteristic property of a variational principle. Equation (114) also shows that the numerical scheme underestimates the matching matrix if W is positive definite.

We shall estimate in the following the convergence rate r,

$$W(\varepsilon, \varepsilon) \equiv \mathcal{O}(M^{2r}) \tag{115}$$

of the finite-element discretization, as the number of radial elements $M \to \infty$. It is well known (see, e.g., [24]) that a linear mesh node distribution gives $r = -1$ for the linear tent functions and $r = -3$ for cubic Hermite elements, provided there is no (radial) singularity. Being confronted with regular singular surfaces at the magnetic axis $\psi_0 = 0$ and at the rational surfaces ψ_i, $i = 1, 2, \ldots, N$, we expect a diminished convergence rate unless the mesh nodes $\psi^{(k)}$, $k = 1, 2, \ldots, M$, are appropriately packed about the ψ_i. This is achieved by means of a mesh–node generating function

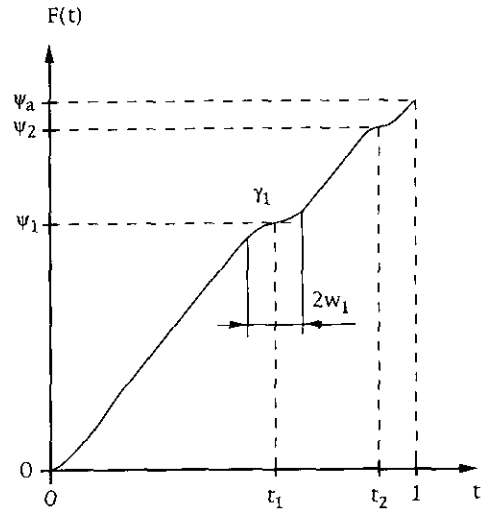

FIG. 4. A mesh generating function which is continuous in value and derivative.

$$F\colon \psi^{(k)} = F(t^{(k)}), \quad t^{(k)} \sim k/M, \tag{116}$$

of the rational index $0 \le t^{(k)} \le 1$, which behaves as

$$F(t^{(k)}) = \psi_i \pm \text{const}|t^{(k)} - t_i|^{\gamma_i} \tag{117}$$

in the vicinity of ψ_i ($t_0 = 0 < t_1 < t_2 \cdots < t_N < 1$), as shown in Fig. 4.

Returning to (115), we find that ε must vanish somewhere between each mesh node in order that (113) hold for $u = e^{(l)}_k$. That is, ε can be bounded in each interval $\psi^{(k)} \le \psi \le \psi^{(k)}$ by

$$\varepsilon \le \tfrac{1}{2}\check{\xi}''_k[\psi^{(k+1)} - \psi^{(k)}]^2$$
$$\varepsilon' \le \check{\xi}''_k[\psi^{(k+1)} - \psi^{(k)}], \tag{118}$$

where

$$\check{\xi}''_k \equiv \max \partial^2_\psi \check{\xi}(\psi, \theta), \quad \psi^{(k)} \le \psi \le \psi^{(k+1)}, 0 \le \theta \le 2\pi, \tag{119}$$

is the maximum value within the slice $(\psi^{(k)}, \psi^{(k+1)})$. Assuming for the moment no singularity so that $|\check{\xi}''_k| < \infty$, we then recover the result

$$W(\varepsilon, \varepsilon) = (\varepsilon', \mathcal{D}_\theta \mathcal{G} \mathcal{D}_\theta \varepsilon') + \cdots = \text{const}\,(\check{\xi}''_{\max})^2 h_{\max}^2 + \mathcal{O}(h_{\max}^3), \tag{120}$$

where $h_{\max} \equiv \max_{k=1,2,\ldots,M-1}(\psi^{(k+1)} - \psi^{(k)}) \propto 1/M$ and $\check{\xi}''_{\max} \equiv \max_{k=1,2,\ldots,M-1}\check{\xi}''_k$, that a linear mesh gives a convergence rate of $r = -1$ and often provides the highest accuracy, since $h_{\max} \propto M^{-1}$ is minimal.

In the presence of singularities, we restrict for simplicity the analysis to the zone $t_i \le t \le t_i + w_i < t_{i+1}$, where the nodes are packed. In the limit of

$$\begin{aligned} M &\to \infty \\ t^{(k)} &\to t = k/M \\ 1/M &\to dt \\ \psi^{(k+1)} - \psi^{(k)} &\to d\psi, \end{aligned} \tag{121}$$

we thus have $d\psi \propto (t - t_i)^{\gamma_i - 1}\, dt$ from (117). The singularity of (17) is simulated by

$$\langle l | \mathcal{D}_\theta \mathcal{G} \mathcal{D}_\theta | l \rangle \propto (\psi - \psi_i)^{\beta_i} \tag{122}$$

vanishing ($\beta_i > 0$) as $\psi \to \psi_i$, for some poloidal modes l. About the rational surfaces $i = 1, 2, \ldots, N$, we take $l = m_i$ and $\beta_i = 2$, whereas $\beta_0 = 1$ for $l \neq 0$ at the magnetic axis $\psi_0 = 0$. Similarly, we have

$$\check{\xi} \propto (\psi - \psi_i)^{\alpha_i} \exp(il\theta) \tag{123}$$

as generic behaviour as $\psi \to \psi_i$: $\alpha_0 = l/2$ ($l \neq 0$) and $\alpha_i = -\frac{1}{2} + \mu_i$ for $i = 1, 2, \ldots, N$, respectively. Introducing (122) and (123) in the expression for W, using (118) and keeping the leading terms in $1/M$, we get

$$\begin{aligned} W(\varepsilon, \varepsilon) &\le \text{const} \int d\psi (\check{\xi}''_{\max})^2 (t - t_i)^{2(\gamma_i - 1)} (dt)^2 (t - t_i)^{\gamma_i \beta_i} \\ &= \text{const}\, \frac{\alpha_i^2 (\alpha_i - 1)^2}{M^2} \int_{t_i}^{t_i + w_i} dt\, t^{2\gamma_i(\alpha_i - 2) + 3(\gamma_i - 1) + \gamma_i \beta_i}. \end{aligned} \tag{124}$$

The matching data error therefore converges as M^{-2} provided integral (124) converges, that is,

$$\gamma_i > \frac{2}{2\alpha_i + \beta_i - 1}. \tag{125}$$

This gives the following minimal mesh scaling:

$$\begin{aligned} \gamma_0 &> 2/l \quad \text{for } l \neq 0 \\ \gamma_0 &= 1 \quad \text{for } l = 0 \end{aligned} \tag{126}$$

at $\psi = 0$, and

$$\begin{aligned} \gamma_i &\ge 1/\mu_i \quad \text{for } \mu_i \neq \tfrac{1}{2}, \tfrac{3}{2} \\ \gamma_i &= 1 \quad \text{for } \mu_i = \tfrac{1}{2}, \tfrac{3}{2} \end{aligned} \tag{127}$$

about ψ_i, $i = 1, 2, \ldots, N$. Note that it is sufficient to take a linear mesh in the pressureless case as $\alpha_i = 0$. It is straightforward to verify that taking l to be non-resonant (e.g., $l = m_i$ so that $\beta_i = 0$ and $\alpha_i = \frac{1}{2} + \mu_i$), yields minimal γ_i which are identical to (126) and (127).

As it is always desirable from an accuracy viewpoint to adopt, whenever possible, a linear mesh we restrict the use of a graded mesh to the immediate vicinities of the singular surfaces ψ_i. To construct the mesh, we therefore divide each section (ψ_i, ψ_{i+1}) into zones; the first zone has a nonuniform node distribution

$$F(t) = \psi_i + \frac{b w_i}{\gamma_i} \left(\frac{t - t_i}{w_i} \right)^{\gamma_i}, \quad t_i \le t \le t_i + w_i, \tag{128}$$

which merges smoothly to the second zone where the node distribution function

$$F(t) = b \left\{ t - \frac{w_0(\gamma_0 - 1)}{\gamma_0} - 2 \sum_{j=1}^{i} \frac{w_j(\gamma_j - 1)}{\gamma_j} \right\}, \quad t_i + w_i \le t \le t_{i+1} - w_{i+1}, \tag{129}$$

is linear. There is a third, graded zone,

$$F(t) = \psi_{i+1} - \frac{b w_{i+1}}{\gamma_{i+1}} \left(\frac{t_{i+1} - t}{w_{i+1}} \right)^{\gamma_{i+1}}, \quad t_{i+1} - w_{i+1} \le t \le t_{i+1}, \tag{130}$$

unless $i = N + 1$ and $\psi_{N+1} = \psi_a$.

In Eqs. (128)–(130), w_i, $i = 0, 1, \ldots, N$, represent the graded-zone width on the t axis (see Fig. 4). It is easy to verify that such a mesh has a smooth node distribution as dF/dt is continuous, with slope

$$b = \psi_a \left\{ 1 - \frac{w_0(\gamma_0 - 1)}{\gamma_0} - 2 \sum_{i=1}^{N} \frac{w_i(\gamma_i - 1)}{\gamma_i} \right\}^{-1} \tag{131}$$

in the linear zone and

$$t_i = \frac{\psi_i}{b} + \frac{w_0(\gamma_0 - 1)}{\gamma_0} + 2 \sum_{j=1}^{i-1} \frac{w_j(\gamma_j - 1)}{\gamma_j} + \frac{w_i(\gamma_i - 1)}{\gamma_i}. \tag{132}$$

Note that $b > 0$ requires, in addition,

$$\frac{w_0(\gamma_0 - 1)}{\gamma_0} + 2 \sum_{i=1}^{N} \frac{w_i(\gamma_i - 1)}{\gamma_i} < 1 \tag{133}$$

which imposes some constraint on the maximum value of the w_i. In order that the distance between t_i and the nearest adjacent node vary smoothly with M, avoiding therefore oscillatory convergence, we introduce the number of nodes

$$M_i \equiv \text{int}[t_i M] \tag{134}$$

up to the rational surface ψ_i ($M_0 = 0$), with int[·], denoting "the closest integer smaller or equal," and set

$$t^{(k)} = \begin{cases} \dfrac{k-1}{M_1} t_1, & i = 0, \\ t_i + \dfrac{k - M_i}{M_{i+1} - M_i + 1}(t_{i+1} - t_i), & i = 1, 2, ..., N \\ t_N + \dfrac{k - M_N}{M - M_N}(1 - t_N), & i = N + 1. \end{cases} \tag{135}$$

XI. NUMERICAL TEST CASES

The PEST-3 code should be regarded as an extension of the ideal stability code PEST-2 based on the scalar form $W(\xi, \xi)$ of the energy functional [13]. Therefore, PEST-3 may also be used for ideal stability computations. The numerical advantages of this approach lie in reduced computing time and memory storage [15]. Compared to other ideal codes such as ERATO [25] and PEST-1, the PEST-2 approach is most appropriate to implement the matching data calculation due to the analytical elimination of the strongly singular $\nabla\psi \times \mathbf{B} \cdot \boldsymbol{\xi}$ displacement [23].

The ideal equilibrium MHD equations are solved numerically using the cubic-Hermite finite element code CHEASE [26] after specifying $p'(\psi)$ and the surface averaged toroidal current density

$$I^* \equiv \frac{\langle\langle \mathbf{J} \cdot \nabla\Phi \rangle\rangle}{\langle\langle 1/R \rangle\rangle}, \tag{136}$$

where

$$\langle\langle \cdot \rangle\rangle \equiv \int_0^{2\pi} d\theta \mathcal{J} \cdot \tag{137}$$

is 2π times the flux surface average and

$$V'(\psi) \equiv \int_0^{2\pi} d\theta \mathcal{J} \tag{138}$$

is the surface of a magnetic tube divided by 2π. We also use the code DMAP to remap equilibrium quantities onto a (ψ, θ) mesh. DMAP generates its own radial mesh which can be either linear in ψ, linear in $\sqrt{\psi}$ (more accurate near $\psi = 0$) or else imports the CHEASE mesh, which may be packed in ψ about any q surface. We found the latter option to have a positive impact on the computation accuracy of the Frobenius coefficients in Sections IV–V. To allow flexibility in the choice of the mesh in θ, we also specify the Jacobian dependence $\mathcal{J} \propto X^i/|\nabla\psi|^j$ by choosing i and j. The combination $i = 1$ and $j = 1$ yields the *equal-arc* coordinate system which has the virtue of possessing the most uniform distribution of nodes in θ [15] and should therefore be preferred.

The outer matching data are determined by studying the convergence in M^{-2} and using linear regression to extrapolate the data to $M \to \infty$. We have taken the range of poloidal modes $l = -8, -5, ..., +8$ for the circular cross section plasmas considered in Section XI.B and Section XI.C, to be symmetric ($|\check{L}| = \hat{L}$) so as to satisfy accurately $(\mathcal{G}^{-1})^{-1} = \mathcal{G}$ of (11). This is important as $\mathcal{G}$ appears in the source term (104) and in its inverse form in the Frobenius expansion (e.g., in (46)], in order for $\hat{\xi}$ and $\hat{\chi}$ to satisfy the approximation condition (15).

A. *Resistive Layer Models*

Although the inherent flexibility of the asymptotic matching method may be utilized to study a large range of non-ideal modes, we restrict ourselves to resistive modes for the sake of validating the outer matching data calculation. We assume the inner layer dynamics to be governed by the GGJ equations. The inner matching data $\Delta(\gamma)$ and $\Delta(\gamma)$, which depend on the set

$$E = -\frac{p'\langle\langle B^2/|\nabla\psi|^2\rangle\rangle}{2\pi q'^2}\left(V'' - \frac{gq'V'}{\langle\langle B^2\rangle\rangle}\right), \tag{139}$$

$$F = \frac{p'^2}{4\pi^2 q'^2}(g^2\langle\langle B^2/|\nabla\psi|^2\rangle\rangle\langle\langle 1/B^2|\nabla\psi|^2\rangle\rangle - g^2\langle\langle 1/|\nabla\psi|^2\rangle\rangle^2 + \langle\langle B^2/|\nabla\psi|^2\rangle\rangle\langle\langle 1/B^2\rangle\rangle), \tag{140}$$

$$H = \frac{gp'}{2\pi q'}\left(\langle\langle 1/|\nabla\psi|^2\rangle\rangle - \frac{\langle\langle B^2/|\nabla\psi|^2\rangle\rangle V'}{\langle\langle B^2\rangle\rangle}\right), \tag{141}$$

$$K = \frac{4\pi^2 q'^2\langle\langle B^2\rangle\rangle}{Mp'^2V'^2\langle\langle B^2/|\nabla\psi|^2\rangle\rangle}, \tag{142}$$

$$G = \frac{\langle\langle B^2\rangle\rangle}{\Gamma pMV'} \tag{143}$$

of quantities defined in Eqs. (13) and (14) of GGJ are computed at each ψ_i, the local ideal and resistive indices reading as

$$\begin{aligned} D_I &= E + F + H - \tfrac{1}{4} \\ D_R &= E + F + H^2. \end{aligned} \tag{144}$$

In the finite β ordering $D_R \sim \hat{Q}^{3/2}$, an analytic expression exists and is given by Eq. (87) in GGJ. For the plasmas consid-

ered in Sections XI.B and XI.C, H can be neglected so that this expression reduces to

$$\Delta_i(\hat{Q}_i) = \frac{2^{2\mu_i}\pi\Gamma(3/4)}{2\mu_i f_i L_i^{2\mu_i}\Gamma(1/4)}\hat{Q}_i^{5/4}\left(1 - \frac{\pi D_{R,i}}{4\hat{Q}_i^{3/2}}\right) \tag{145}$$

in each layer, $i = 1, 2, ..., N$, where

$$\hat{Q}_i \equiv \gamma/Q_i \tag{146}$$

is the normalized growth rate,

$$Q_i \equiv \left(\frac{4\pi^2\eta n^2 q_i'^2\langle\langle B^2\rangle\rangle}{V'^2\rho M\langle\langle B^2/|\nabla\psi|^2\rangle\rangle}\right)^{1/3} \tag{147}$$

is the typical resistive growth rate $\sim\eta^{1/3}$,

$$M \equiv \frac{\langle\langle B^2/|\nabla\psi|^2\rangle\rangle}{V'^2}(\langle\langle|\nabla\psi|^2/B^2\rangle\rangle + g^2[\langle\langle 1/B^2\rangle\rangle - V'^2/\langle\langle B^2\rangle\rangle]), \tag{148}$$

a factor which is equal to one in the cylindrical limit.

The growth rates γ are obtained by substituting the submatrix Δ' into the tearing dispersion relation (87) and searching for the dominant root in the complex growth rate plane using the DISP code, with

$$L_i \equiv \left(\frac{\rho M\eta^2\langle\langle B^2\rangle\rangle^2 V'^2}{4\pi^2 n^2 q_i'^2\langle\langle B^2/|\nabla\psi|^2\rangle\rangle^2}\right)^{1/6} \tag{149}$$

as the inner layer width $\sim\eta^{1/3}$. The growth rate so obtained is then compared with the γ computed by the full resistive MARS code. The influence of the inverse aspect ratio $\varepsilon \equiv a/R_0$ on stability is studied, keeping the Lundquist number

$$S \equiv \frac{a^2 B_0}{\sqrt{\rho}R_0\eta} \tag{150}$$

constant. (In (150), a is the minor radius, R_0 is the major radius, B_0 is the magnetic field on axis, and ρ is the density which we take constant and equal to one.)

B. $\beta = 0$ *Resistive Kink*

We start with the pressureless, $n = 1$ internal (fixed boundary conditions $\xi(\psi_a) = 0$) kink mode in a circular cross section plasma with equilibrium profiles described by Fig. 1 in Bondeson, Vlad, and Lütjens [6] (henceforth referred to as BVL). The surface-averaged current density I^* is expressed as a quadratic polynomial in $\sqrt{\psi}$ between $\psi = 0$ and $\psi = 0.25\psi_a$, with non-zero slope at the origin and zero slope at the "knee" $0.25\psi_a$, after which I^* falls rapidly to vanish at $\psi = \psi_a$, the flattened profile of I^* ensuring that q' remains modest at the rational surface $\psi_1 = 0.16\psi_a$, where $q = 1$.

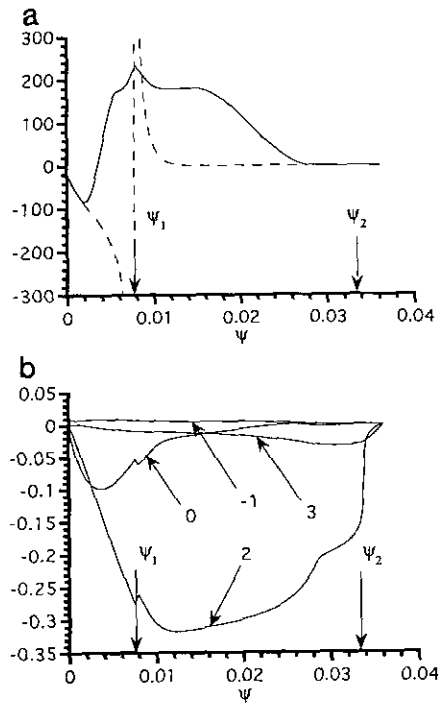

FIG. 5. (a) Response function $\langle 1|\xi_{(1-)}\rangle$ for the zero pressure, fixed boundary plasma with inverse aspect ratio $\varepsilon = 0.3$. The fundamental solution ξ_{1-}, which exhibits the resistive kink behaviour, is shown in dashed line. Note the $\xi \sim \sqrt{\psi}$ behaviour on the axis. (b) Non-resonant $l \neq m_1$ Fourier components of $\xi_{(1-)}$. The presence of a $q = 2$ rational surface near the plasma edge is responsible for the quantum jump of $\langle 2|\xi_{(1-)}\rangle$ at $\psi \approx 0.034$.

Following our prescriptions (126) and (127), we take uniformly distributed mesh nodes $\gamma_i = 1$, $i = 1, 2, ..., N$ about the rational surfaces and $\gamma_0 = 2$ about $\psi = 0$. The response function $\xi_{(1-)}$ driven by a tearing parity $\hat{\xi}$ located at the $q = 1$ surface is shown in Fig. 5 for an inverse aspect ratio $\varepsilon = 0.3$. The quantity Δ'_{11} is given by the jump (89) of the response at the $q = 1$ surface, which is difficult to estimate here due to inaccuracies associated with rapid variations of equilibrium quantities, an instance where the computation of the matching data using the GGF scheme is the sole alternative (see Fig. 6). The inaccuracy of the response about the $q = 1$ surface is also perceptible among non-resonant modes, which should be continuous in values and discontinuous in derivatives. The off-diagonal element Δ'_{21} can, however, be estimated from the jump of $\langle 2|\xi_{1-}\rangle$ at the $q = 2$ surface to be approximately 0.18. This is in rough agreement with the value of 0.23 found by using the GGF method and extrapolating to $M \to \infty$.

Figure 6 illustrates the convergence of the dominant (a) and subdominant (b) eigenvalues of the Δ' matrix for a prescribed solution covering $\delta_b = 80\%$ of the distance between rational surfaces, with $M = 160, 180, 200, 220, 240, 260, 280$, and 299. The dominant eigenvalue λ_1 possesses a smooth convergence

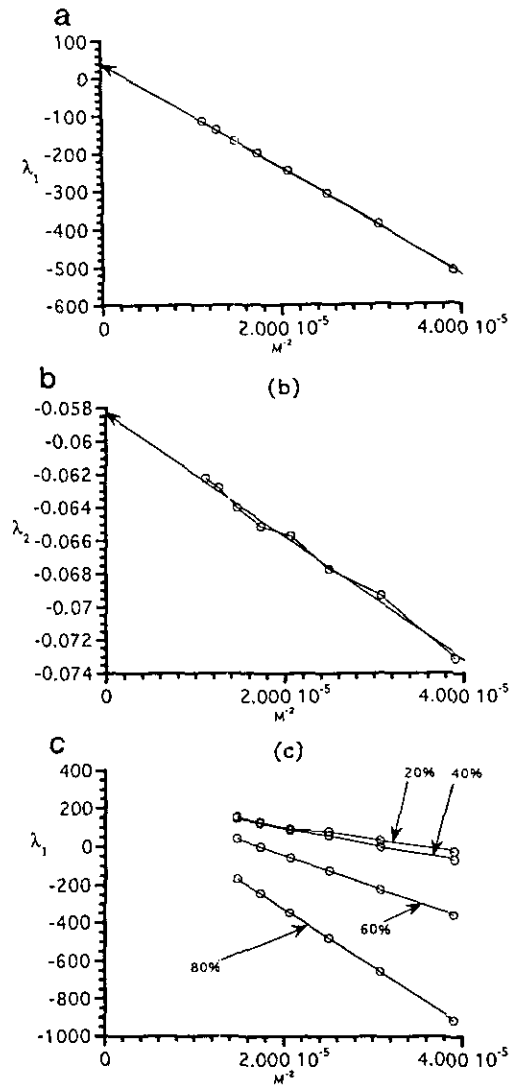

FIG. 6. Convergence of the dominant (a) eigenvalue λ_1 and the subdominant (b) eigenvalue λ_2 of Δ' versus the inverse square of the number of radial mesh nodes M = 160, 180, 200, ···, 280, 299, for the pressureless, fixed boundary case at inverse aspect ratio $\varepsilon = 0.3$. The extrapolated values to $M \to \infty$ are $\lambda_1 \to 43.2$ and $\lambda_1 \to -0.0581$. (c) Effect of the normalized prescribed solution support δ_b = 80%, 60%, 40%, and 20% on the convergence properties for $\varepsilon = 0.2$.

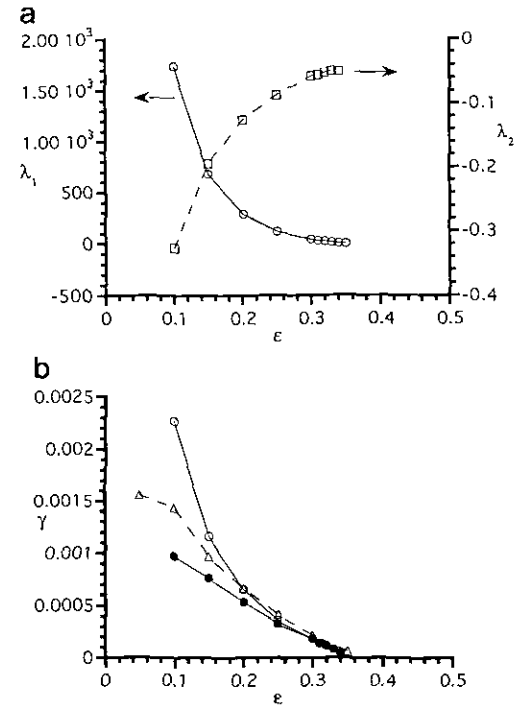

FIG. 7. Fixed boundary plasma at zero pressure and $S = 10^6$. (a) Dominant and recessive eigenvalues versus inverse aspect ratio ε. (b) Comparison of computed growth rates γ versus inverse aspect ratio ε, using the code PEST-3 (solid lines) and the code MARS (dashed line). Two analytic expressions for the inner Δ are adopted: with (closed symbols) or without the pole (open symbols) at $\hat{Q} = 1$.

behaviour, allowing for precise extrapolation to infinite M to yield the unstable value of 43.2, which is found to be essentially identical to Δ'_{11} ($M \to \infty$). The convergence of the second eigenvalue λ_2 slightly suffers, by exhibiting some wiggling behaviour, due to the proximity of the $q = 2$ surface from ψ_a ($\psi_2 \approx 0.93\psi_a$) so that only up to 20 nodes are present in the section (ψ_2, ψ_a). The extrapolated value $\lambda_2 \approx -0.0581$ being negative and approximately equal to Δ'_{22}, we deduce that the dominant mode is $m = 1, n = 1$ kink, with negligible coupling from the stable $q = 2$ surface. As one approaches the ideal marginal stability point by decreasing ε, the slope of the convergence in M^{-2} becomes steeper. This effect is shown in Fig. 6(c) for $\varepsilon = 0.2$. Nevertheless, the convergence behaviour can be flattened by reducing the magnitude of the prescribed energy in (99). This is achieved by limiting the extension of the shape functions H_i of Fig. 2, at the cost of a slight deterioration of the convergence behaviour which becomes noticeable for $\delta_b = 20\%$.

The resistive kink mode is known to be ideally marginal stable ($\Delta' \to \infty$) in the limit of the inverse aspect ratio $\varepsilon \to 0$. As ε increases, λ_1 decreases to become negative (stable) at moderate $\varepsilon \approx 0.35$. Figure 7 shows good agreement between the stability limit $\varepsilon \approx 0.35$ computed by PEST-3 and MARS (Fig. 2 in BVL). Comparing the growth rates for $S = 10^6$ by matching Δ' to the inner data (145) (and setting $D_R = 0$), we note, however, a discrepancy arising at larger γ's. This is mainly attributed to the approximate form of (145) which, in particular, does not account for the presence of a pole at $\hat{Q}_i = 1$:

$$\Delta_i(\hat{Q}_i) = \frac{2\pi\Gamma(\frac{3}{4} + \frac{1}{4}\hat{Q}_i)}{2\mu_i f_i L_i(1 - \hat{Q}_i^3)\Gamma(\frac{1}{4} + \frac{1}{4}\hat{Q}_i)}\hat{Q}_i^{5/4} \qquad (151)$$

(written here in its $\beta = 0$ form). This expression is due to Rosenau [27]. In the small γ limit where the correction of (151)

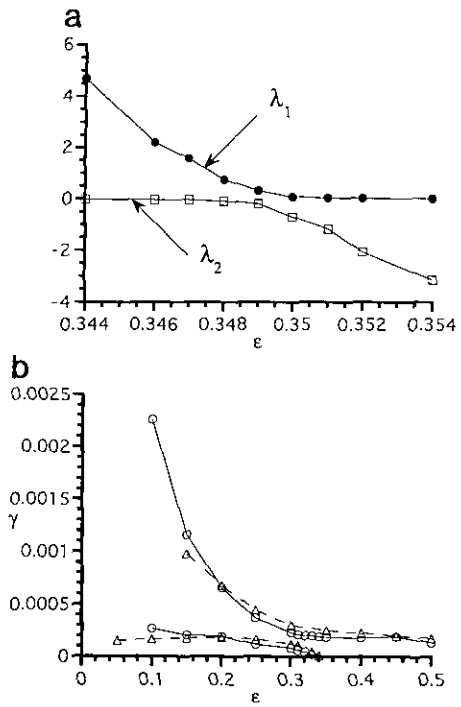

FIG. 8. (a) Details of the mode conversion about $\varepsilon = 0.35$. The mode with eigenvalue λ_1 changes character from internal $q = 1$ to external $q = 2$ and *vice versa* for λ_2. (b) Comparison of computed growth rates versus inverse aspect ratio ε, using the PEST-3 (solid line) and MARS (dashed line) codes for the free-boundary, pressureless plasma at $S = 10^6$.

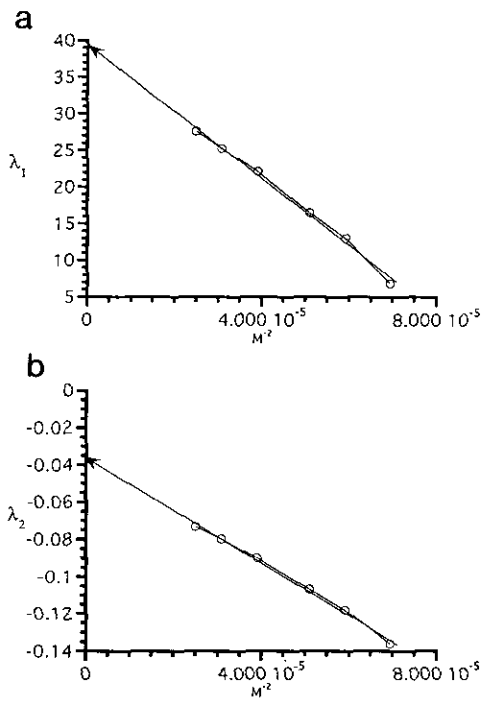

FIG. 9. Convergence of the two eigenvalues λ_1 and λ_2 of Δ' versus the inverse square of the number of radial mesh nodes $M = 120, 130, 140, 160, 180, 200$ for the finite pressure, fixed boundary case at inverse aspect ratio $\varepsilon = 0.35$. The extrapolated values to $M \to \infty$ are $\lambda_1 \to 39.3$ and $\lambda_2 \to -0.036$.

to (145) is negligible, we find the PEST-3 and MARS growth rates to coincide.

The $m = 2$ mode becomes unstable by applying free boundary conditions at a distance $b = 1.2$ times the minor radius a, thus changing the picture from Fig. 7(b) to Fig. 8(b) (Fig. 3(a) in BVL), the $q = 1$ mode remaining largely unaffected. In the intermediate range, $0.3 < \varepsilon < 0.4$, the $m = 2$ and $m = 1$ modes couple through the off-diagonal terms of Δ', e.g., at $\varepsilon = 0.3$,

$$\Delta' = \begin{pmatrix} 43.23 & 0.2298 \\ 0.2298 & -0.05865 \end{pmatrix}, \tag{152}$$

which yields two positive eigenvalues 43.6 and 0.00405 corresponding to the two unstable branches. At $\varepsilon \approx 0.35$, the eigenvalues of Δ' are shown in Fig. 8(a) to collide (mode conversion); λ_1 changes character from an internal kink to become a $q = 2$ mode and *vice versa* for λ_2, as ε increases.

C. *Resistive Stability at Finite* β

We next consider pressure effects on the stability of the fixed boundary plasma of Section XI.B. The equilibrium has the same profile for I^* as for the $\beta = 0$ case but the pressure is finite. The poloidal β,

$$\beta_p \equiv -\frac{4}{I_\Phi^2 R_0} \int_0^\psi dt\, V(t) p'(t) \tag{153}$$

at the $q = 1$ surface, is held fixed, $\beta_p(\psi_1) = 0.05$, as the inverse aspect ratio ε varies. Here, I_Φ is the toroidal current flowing through a $\psi = \text{const}$ surface.

There are two rational surfaces for $\varepsilon \leq 0.45$ and three rational surfaces for $\varepsilon = 0.5$. The $q = 1$ surface is characterized by $\mu < \frac{1}{2}$ so that the response (small) solution is unbounded there. This case is therefore numerically more demanding than the zero-β case; it requires a mesh node packing with exponent $2 < \gamma_i \approx 1/\mu_i \leq 2.3$ in Eqs. (128)–(130). Only one resonant and non-resonant Frobenius order are required in the expansion of $\hat{\xi}_\pm$ and $\hat{\chi}_\pm$ according to (69).

The pressure gradient effects are weak ($0.5 < \mu < 0.508$) at the outer $q = 2$ and $q = 3$ rational surfaces. The nodes must nevertheless be packed; to do so we set $\gamma_2 = \gamma_3 = 2$ constant across the ε range. Two Frobenius orders are needed to represent the prescribed solutions there. To minimize the weight of the prescribed energy in (99), and therefore also the slope of the data convergence in M^{-2}, the large contribution from the first-order Frobenius coefficient is subtracted by using transformation (101) and setting $s_{i-} = -\langle m_i | \xi_1^{(b)} \rangle$, $i = 2, 3$. The convergence of the two eigenvalues of the matrix of small to big coefficients Δ' is shown in Fig. 9 for $\varepsilon = 0.35$. The inner

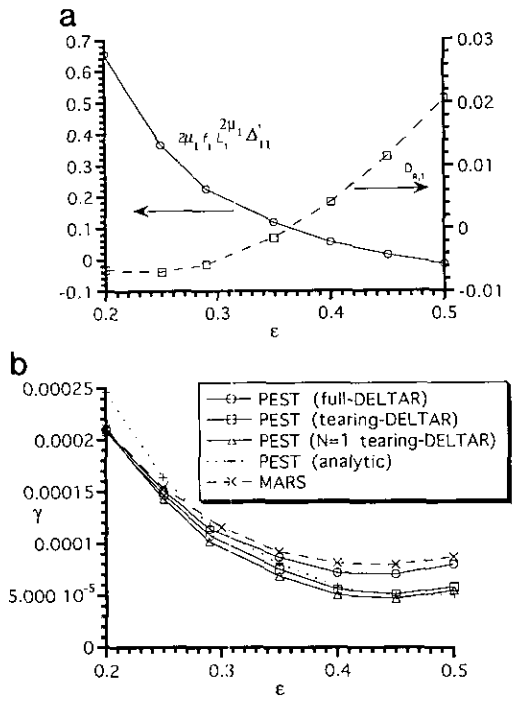

FIG. 10. Fixed boundary plasma at finite pressure and $S = 10^7$. (a) Non-dimensional outer matching data $2\mu_1 f_1 L_1^{2\mu_1}\Delta'_{11}$ (left ordinate axis) and resistive interchange index $D_{R,1}$ versus inverse aspect ratio ε. (b) Comparison of computed growth rates γ versus inverse aspect ratio ε, using the code PEST-3 coupled to the DELTAR code (solid lines), the code PEST-3 coupled to inner analytic $\mathbf{\Delta}$ (dotted line) and the code MARS (dashed line). The discrepancies arising from matching $\mathbf{D}'$ to $\mathbf{D}$ (circles), $\mathbf{\Delta}'$ to $\mathbf{\Delta}$ (squares), and Δ'_{11} to $\Delta_1/2\mu_1 f_1 L_1^{2\mu_1}$ (triangles) are illustrated.

matching data $A(\gamma)$ and $\Delta(\gamma)$ are determined numerically using the code DELTAR [20].

Similarly to the zero-β case, the instability is essentially a tearing mode driven by $\Delta'_{11} > 0$ at low inverse aspect ratio ε. The tearing mode is stabilized at $\varepsilon \approx 0.45$, where the mode changes character to become resistive interchange. Figure 10(a) exhibits the decrease of $2\mu_1 f_1 L_1^{2\mu_1}\Delta'_{11}$, and the simultaneous emergence of a resistive interchange instability $D_{R,1} > 0$ as ε increases. The resistive interchange growth rate can easily be estimated by requiring the term in parenthesis in (145) to vanish: $\gamma \approx Q_1(\pi D_{R,1}/4)^{2/3}$ for $D_{R,1} > 0$ and $2\mu_1 f_1 L_1^{2\mu_1}\Delta'_{11} \approx 0$ to give $\gamma \approx 5.67 \times 10^{-5}$ at $\varepsilon = 0.5$, in agreement with the corresponding value in Fig. 10(b). The various contributions in the dispersion relations (84)–(85) are analyzed in Fig. 10(b) (the MARS growth rates are taken from Fig. 6(a) in BVL). We find the coupling of $q = 1$ to $q = 2$ and $q = 3$ rational surfaces to be weakly destabilizing. As for the zero-β case in Section XI.B, neglecting the pole in the analytic approximation (145) of $\Delta(\gamma)$ is also destabilizing, particularly for large growth $\gamma > 5 \times 10^{-5}$. The most important effect, however, is due to the lifting of the "constant Ψ" approximation, which is accomplished here by taking into account the full dispersion relation involving tearing and interchange parity modes (i.e., taking (84) rather than (87)).

XII. CONCLUSIONS

We have discussed in this paper, the development of the MHD stability code PEST to allow computation of tearing and resistive interchange modes by determining the matching data in the outer region. The code has proven to have robust convergence properties: quadratic convergence holds, provided the mesh is packed about the rational surfaces (in the finite β case). We have also given indications how to control the convergence slope when the response and the prescribed energies have approximately the same but opposite magnitudes so that large cancellations occur, by varying the size of the prescribed solution supports. In general we take the supports to cover a large fraction of the distance between neighbouring rational surfaces (e.g., 80%) as this provides the smoothest convergence. Steep convergence may also arise when μ slightly exceeds $\frac{1}{2}$, we then advise subtracting the "polluting" small solution component from the prescribed solution.

It is, to our knowledge, the first time that the validity of the asymptotic matching method and, in particular, the GGJ inner layer model, could be tested directly against a code making no assumption as to the growth rate scaling, the resistive layer width, etc. Agreement between the growth rates computed by MARS and PEST-3 are satisfactory to very satisfactory, suggesting that the matching data computation is accurate and gives accurate resistive growth rates when $S \geq 10^6$.

As for the numerical advantages of the PEST approach in terms of memory storage and execution time, we find the comparison to apply on a CRAY-YMP computer,

	M Words	*CPU seconds*
PEST-3:	1.5 (2.1)	9 (13)
MARS:	7.5	36

(154)

for a typical fixed boundary plasma possessing two rational surfaces, using $M = 150$ radial elements and 10 Fourier modes (respectively, 20 Fourier modes), to which it should be added that the PEST data concern the outer matching data computation only. Furthermore, contrary to the present PEST version, MARS does not assume up–down symmetric plasmas. The data in parenthesises thus anticipate the memory and time requirements of an up-down asymmetric version of PEST for this case.

PEST's reduced numerical needs make the extension of the formulation to three-dimensional plasmas attractive. This can be achieved by modifying existing three-dimensional, ideal stability codes which use Fourier decomposition in the poloidal and toroidal directions. The resulting distribution of rational surfaces (which formally become dense as the number of Fourier mode goes to infinity) may, however, in some cases pose a

problem, especially when the support of the prescribed elements shrinks excessively.

At present, the formulation has been implemented for $\mu < 1$ ($-1 < D_I < 0$). It can be envisaged to extend the limit to μ exceeding one, although this ultimately addresses issues about the smoothness of the equilibrium quantities. On the other hand, stabilization by favourable curvature ($D_R < 0$) would become so effective that resistive modes are practically eliminated at large S. The limitation $\mu < 1$ is, therefore, not as restrictive as it may first appear: all the interesting physics is expected to take place in the regime of low β and small D_R, where resistive MHD modes are relevant.

APPENDIX A: PARITY OF THE GENERALIZED FUNCTIONS x^α

Although x^α admits in general the even and odd parities, we will see that only one parity survives for particular values of α. To do so we turn to the one-dimensional version of (17),

$$\frac{d}{dx}x^2\frac{d}{dx}y(x) - gy(x) = 0 \tag{A1}$$

with $x \equiv \psi - \psi_i$ and assume g to be, for simplicity, constant. We use the Fourier–Laplace method

$$y(x) = \int_\Gamma \frac{dk}{2\pi}\exp(ikx)y(k), \tag{A2}$$

a natural way to introduce generalized functions, and seek solutions of (A1)

$$k\frac{d^2}{dk^2}ky(k) - gy(k) = 0 \tag{A3}$$

in the k space, where the contour Γ in (A2) is chosen so as to have a vanishing integrand at the end points. The solutions of (A3) have the same form as in x space; that is,

$$y_\pm(k) = k^{\alpha_\pm} \tag{A4}$$

with $\alpha_\pm = -\frac{1}{2} \pm \sqrt{1/4 + g} \equiv -\frac{1}{2} \pm \mu$.

Consider first the case where α is non-integer so that $y(k)$ has a branch line in k space. Different contours are chosen according to whether x is positive or negative. For $x > 0$, the branch line lies on the Im $k > 0$ axis. The contour Γ is broken up into three integrals circumscribing the branchline: a line along the Re $k < 0$ side of the imaginary axis $(-0 + i\infty, -0)$, an asymptotically small circle $(-0, +0)$ rotating counterclockwise about $k = 0$, and a line along the Re $k > 0$ side of the imaginary axis $(+0, +0 + i\infty)$, as shown in Fig. 11. Since the small circle does not contribute for $\alpha = \alpha_+$, we find in this case that

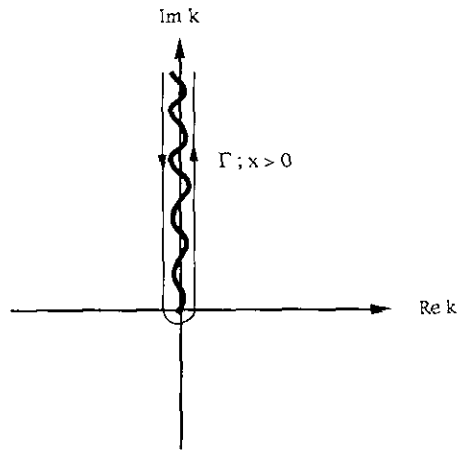

FIG. 11. Integration contour Γ circumscribing the branch line on the Im $k > 0$ axis for $x > 0$.

$$\begin{aligned} y_+(x) &= \int_{-0+i\infty}^{-0}\frac{dk}{2\pi}\exp(ikx)k^{\alpha_-} + \exp(i2\pi\alpha_+) \\ &\quad\times\int_{+0}^{+0+i\infty}\frac{dk}{2\pi}\exp(ikx)k^{\alpha_+} \\ &= \exp(-i\pi\alpha_+/2)x^{-1-\alpha_+}/\Gamma(-\alpha_+), \quad x > 0, \end{aligned} \tag{A5}$$

yields the big solution in x space (times an arbitrary phase factor) since we have $\alpha^{(b)} = -1 - \alpha_+$. Similar expressions to (A5) can be found for $x < 0$ by taking the branch line and Γ to lie in the lower, Im $k < 0$ half-plane. However, it is readily seen that (A5) has a pole at $\alpha_+ = 0, 1, 2, \ldots$ so that k^{α_-} *cannot* generate the big solution *if* α_+ is *integer;* instead $\int(dk/2\pi)\exp(ikx)k^n = (-i)^n\delta^{(n)}(x)$ engenders the nth derivative of the δ function, a solution which does not belong to the outer region. The reason for this is that k^α are not the only solutions of (A3) in the generalized function sense; we find that for the special values of $g = n(n+1) = 0, 2, 6$, etc. ($\mu = 1/2, 1, 3/2$, etc.) we have

$$\begin{matrix} -i\pi k^n \operatorname{sgn} k \\ k^n\delta(k). \end{matrix} \tag{A6}$$

The second solution only contributes in (A2) when $n = 0$, where it gives rise to the constant shift of the small solution. The big solution derives from inserting $-i\pi k^n \operatorname{sgn} k$ in (A2) and integrating along the real axis, which yields

$$\begin{aligned} y^{(b)}(x) &= (-i)^n\frac{d^n}{dx^n}\int_{-\infty}^{\infty}\frac{dk}{2\pi}\exp(ikx)(-i\pi\operatorname{sgn} k) \\ &= i^n n! x^{-n-1}. \end{aligned} \tag{A7}$$

To extract the k^{α_-} solution we proceed cautiously as the integral (A2) diverges at $k = 0$ if $\alpha_- < -1$. Assuming α_- to be within the strip $-n - 1 < \alpha_- < -n$, we integrate n times (A2) by parts,

$$y_-(x) = (-1)^n \frac{\Gamma(\alpha_- + 1)}{\Gamma(\alpha_- + n + 1)} \int_\Gamma \frac{dk}{2\pi} k^{\alpha_- + n} \frac{d^n}{dk^n} \exp(ikx) \qquad \text{(A8)}$$

$$= \exp(-i\pi\alpha_-/2) x^{-1-\alpha_-}/\Gamma(-\alpha_-), \quad x > 0,$$

to recover the small solution in x space. In the limit of $\alpha_- \to -n$ we find that $\int (dk/2\pi) \exp(ikx) k^{-n}$ yields $\delta(x)$ for $n = 0$ and the residue $i^n x^{n-1}/(n-1)!$ for $n \geq 1$, the latter depending on the sign of x through the choice of contour Γ so that the left- and right-sided small solutions are independent *for all* α_-.

We therefore find that the small solution always involves both the even and odd parities but the big solution has definite parity when $\mu = \frac{1}{2}, 1, \frac{3}{2} \ldots$; i.e., x^{-2n} is even and x^{-2n-1} is odd. This result is in agreement with Gel'fand and Shilov [17] who introduce a "regularization" for the singular functions x^α when $\alpha < -\frac{1}{2}$. This regularization, however, presents a pole at $\alpha = -1, -2, \ldots$ and is therefore not properly defined for these values. A judicious choice of parity, however, can cancel the pole and it is found that x_p^{-2n} ($n = 1, 2, \ldots$) is well defined for $p = +$ and similarly x_p^{-2n-1} for $p = -$.

A similar Fourier space analysis of a zero-β, asymmetric inner layer model confirms the suppression of the even big solution at $\mu = \frac{1}{2}$, and has led Dewar and Persson [8] to introduce an inverse formulation in which the small solutions are regarded as driving the big solutions. Then the cases $\mu = \frac{1}{2}, 1, \frac{3}{2}, \ldots$ do not have to be treated as totally distinct cases as they do not give rise to divergent responses. The inverse formulation would probably also be beneficial for treating the small aspect ratio limit of the internal kink mode and other cases close to ideal stability.

ACKNOWLEDGMENTS

This work was partly supported by the Swiss National Science Foundation. One of us, A.P., would like to thank Dr. A. H. Glasser for making the DELTAR code available.

REFERENCES

1. D. C. Robinson and K. McGuire, *Nucl. Fusion* **19,** 115 (1979).
2. B. Kadomstev, *Sov. J. Plasma Phys.* **1,** 389 (1975).
3. J. Kevorkian and J. Cole, *Perturbation Methods in Applied Mathematics* (Springer, Verlag, New York, 1981).
4. H. P. Furth, J. Killeen, and M. N. Rosenbluth, *Phys. Fluids* **6,** 459 (1963).
5. A. H. Glasser, J. M. Greene, and J. L.Johnson, *Phys. Fluids* **18,** 875 (1975).
6. A. Bondeson, G. Vlad, and H. Lütjens, *Phys. Fluids B* **4,** 1889 (1992).
7. R. Fitzpatrick, R. J.Hastie, T. J. Martin, and C. M. Roach, Technical Report No. AEA FUS 224, AEA Fusion, Culham Laboratory Abington, Oxen. OX14 3DB, UK (unpublished).
8. R. L. Dewar and M. Persson, *Phys. Fluids B,* December 1993; ANU/TPP93/, Australian National University, Canberra, ACT 0200, Australia.
9. J. Manickam, R. C. Grimm, and R. L. Dewar, in *Energy Modeling and Simulation,* edited by A. Kydes *et al.* (North–Holland, Amsterdam, 1983), p.355.
10. A. D. Miller and R. L. Dewar, *J. Comput. Phys.* **66,** 356 (1986).
11. A. Pletzer and R. L. Dewar, *J. Plasma Phys.* **45,** 427 (1991).
12. W. A. Newcomb, *Ann. Phys. (N.Y.)* **10,** 232 (1960).
13. I. B. Bernstein, E. A. Frieman, M. D. Kruskal, and R. M. Kulsrud, *Proc. Roy. Soc. A* **244,** 17 (1958).
14. M. Bineau, *Nucl. Fusion* **2,** 130 (1962).
15. R. C. Grimm, R. L. Dewar, and J. Manickam, *J. Comput. Phys.* **49,** 94 (1983).
16. R. L. Dewar, D. A. Monticello, and W. N.-C. Sy, *Phys. Fluids* **27,** 1723 (1984).
17. I. M. Gel'fand and G.E. Shilov, *Generalized Functions* (Academic Press, New York, 1964).
18. R. L. Dewar and A. Pletzer, *J. Plasma Phys.* **43,** 291 (1990).
19. E. L. Ince, *Ordinary Differential Equations* (Dover, New York, 1956).
20. A. H. Glasser, C. C. Jardin, and G. Tesauro, *Phys. Fluids* **27,** 1225 (1984).
21. P. M. Morse and H. Feshbach, *Methods of Theoretical Physics* (McGraw–Hill, New York, 1953).
22. A. Pletzer, Ph.D. thesis, Australian National University, Canberra, ACT 0200, Australia, 1992.
23. M. S. Chu, R. L. Dewar, J. M. Greene, and A. Pletzer, *Phys. Fluids B* **5,** 1593 (1993).
24. K. W. Morton, in *Finite Elements in Physics,* edited by R. Gruber (North-Holland, Amsterdam, 1987), p. 1.
25. R. Gruber *et al., Comput. Phys. Commun.* **21,** 323 (1981).
26. H. Lütjens, A. Bondeson, and A. Roy, *Comput. Phys. Commun.* **69,** 287 (1992).
27. P. Rosenau, *Phys. Fluids* **26,** 2578 (1983).